Inorganic Chemistry

Article

pubs.acs.org/IC

π-Expansive Heteroleptic Ruthenium(II) Complexes as Reverse Saturable Absorbers and Photosensitizers for Photodynamic Therapy

Li Wang,[†] Huimin Yin,[‡] Mohammed A. Jabed,[†] Marc Hetu,[‡] Chengzhe Wang,[†] Susan Monro,[‡] Xiaolin Zhu,[†] Svetlana Kilina,[†] Sherri A. McFarland,*[,‡,§] and Wenfang Sun*[,†]

[†]Department of Chemistry and Biochemistry, North Dakota State University, Fargo, North Dakota 58108-6050, United States

[‡]Department of Chemistry, Acadia University, 6 University Avenue, Wolfville, NS B4P 2R6, Canada

[§]Department of Chemistry and Biochemistry, University of North Carolina at Greensboro, Greensboro, North Carolina 27402-6170, United States

Supporting Information

ABSTRACT: Five heteroleptic tris-diimine ruthenium(II) complexes $[RuL(N^N)_2](PF_6)_2$ (where **L** is 3,8-di(benzothiazolylfluorenyl)-1,10-phenanthroline and N^N is 2,2′-bipyridine (bpy) (**1**), 1,10-phenanthroline (phen) (**2**), 1,4,8,9-tetraazatriphenylene (tatp) (**3**), dipyrido[3,2-*a*:2′,3′-*c*]phenazine (dppz) (**4**), or benzo[*i*]dipyrido[3,2-*a*:2′,3′-*c*]phenazine (dppn) (**5**), respectively) were synthesized. The influence of π-conjugation of the ancillary ligands (N^N) on the photophysical properties of the complexes was investigated by spectroscopic methods and simulated by density functional theory (DFT) and time-dependent DFT. Their ground-state absorption spectra were characterized by intense absorption bands below 350 nm (ligand **L** localized $^1\pi,\pi^*$ transitions) and a featureless band centered at ∼410 nm (intraligand charge transfer (^{1}ILCT)/$^1\pi,\pi^*$ transitions with minor contribution from metal-to-ligand charge transfer (^{1}MLCT) transition). For complexes **4** and **5** with dppz and dppn ligands, respectively, broad but very weak absorption (ε < 800 M^{-1} cm^{-1}) was present from 600 to 850 nm, likely emanating from the spin-forbidden transitions to the triplet excited states. All five complexes showed red-orange phosphorescence at room temperature in CH_2Cl_2 solution with decreased lifetimes and emission quantum yields, as the π-conjugation of the ancillary ligands increased. Transient absorption (TA) profiles were probed in acetonitrile solutions at room temperature for all of the complexes. Except for complex **5** (which showed dppn-localized $^3\pi,\pi^*$ absorption with a long lifetime of 41.2 μs), complexes **1**−**4** displayed similar TA spectral features but with much shorter triplet lifetimes (1−2 μs). Reverse saturable absorption (RSA) was demonstrated for the complexes at 532 nm using 4.1 ns laser pulses, and the strength of RSA decreased in the order: **2** ≥ **1** ≈ **5** > **3** > **4**. Complex **5** is particularly attractive as a broadband reverse saturable absorber due to its wide optical window (430−850 nm) and long-lived triplet lifetime in addition to its strong RSA at 532 nm. Complexes **1**−**5** were also probed as photosensitizing agents for in vitro photodynamic therapy (PDT). Most of them showed a PDT effect, and **5** emerged as the most potent complex with red light (EC_{50} = 10 μM) and was highly photoselective for melanoma cells (selectivity factor, SF = 13). Complexes **1**−**5** were readily taken up by cells and tracked by their intracellular luminescence before and after a light treatment. Diagnostic intracellular luminescence increased with increased π-conjugation of the ancillary N^N ligands despite diminishing cell-free phosphorescence in that order. All of the complexes penetrated the nucleus and caused DNA condensation in cell-free conditions in a concentration-dependent manner, which was not influenced by the identity of N^N ligands. Although the mechanism for photobiological activity was not established, complexes **1**−**5** were shown to exhibit potential as theranostic agents. Together the RSA and PDT studies indicate that developing new agents with long intrinsic triplet lifetimes, high yields for triplet formation, and broad ground-state absorption to near-infrared (NIR) in tandem is a viable approach to identifying promising agents for these applications.

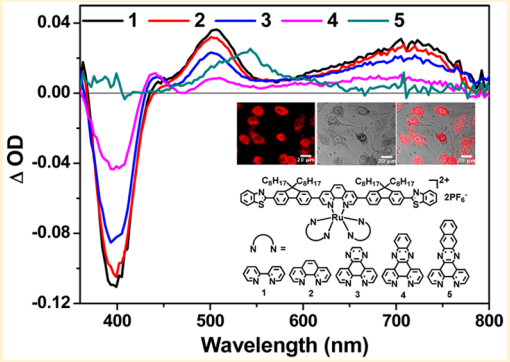

INTRODUCTION

Pseudo-octahedral d^6 Ru(II) polypyridyl complexes have been intensively investigated in recent decades due to their excellent chemical stability,[1] favorable redox properties,[2,3] strong luminescence,[4,5] and relatively long-lived triplet excited states.[6] These properties make Ru(II) complexes ideal candidates for applications in dye-sensitized solar cell,[7,8] catalysis,[9,10] sensing,[11,12] organic light-emitting diode (OLED) displays,[13] biotechnology,[14,15] nonlinear optics (NLO),[16] and photodynamic therapy (PDT).[17−21] Part of their attractiveness for these applications lies in the ease with which their chemical and

Received: October 27, 2016
Published: March 6, 2017

DOI: 10.1021/acs.inorgchem.6b02624
Inorg. Chem. 2017, 56, 3245−3259

photophysical properties can be tuned by judicious choice of the ligands that make the coordination sphere. We have previously exploited this inherently modular architecture to produce π-expansive Ru(II) metal−organic dyads that are characterized by prolonged triplet excited-state lifetimes (>200 μs at 298 K) and very potent in vitro PDT effects.[22] π-Extended ligands also impart a high degree of electron delocalization that facilitates polarization of the electron cloud and enhances the NLO responses in Ru(II) complexes.[23] Because long-lived triplet excited states are desirable for both PDT and reverse saturable absorption (RSA), areas that we are actively investigating, we have begun to develop new complexes for these applications in tandem.[24] While the applications themselves are distinct, there are common requirements for both applications, such as high triplet quantum yields, long-lived triplet excited states, and broad ground-state absorption into the near-infrared (NIR). Thus, there is no logical reason to segregate the development of Ru(II) complexes for both applications.

Ru(II) Complexes as Reverse Saturable Absorbers. Although Ru(II) complexes have been investigated extensively for their second- and third-order NLO properties,[16,25−28] there are limited reports on their use for RSA.[29] Briefly, RSA refers to a nonlinear absorption phenomenon whereby the excited-state absorption cross section of the molecule is larger than that of the ground state. Molecules that demonstrate RSA are highly desirable for applications involving optical switching,[30] laser mode locking,[31] spatial light modulation,[32] and laser beam compression.[33] An ideal broadband reverse saturable absorber should have weak and broad ground-state absorption, while intense excited-state absorption in the visible to the NIR region; long-lived triplet excited states; and high quantum yields for triplet state formation.[34] To the best of our knowledge, the only RSA-related study involving Ru(II) complexes was reported by Humphrey and co-workers.[29] Their hetero-bimetallic Ru(II)/Ir(III) complex behaved primarily as a two-photon absorber under femtosecond excitation at 800 nm and as a reverse saturable absorber under nanosecond excitation at 532 nm. To date, there have been no reports on Ru(II) complexes as broadband reverse saturable absorbers, and thus an understanding of the structure−property correlations for rational design of Ru(II) complexes with broadband and enhanced RSA is lacking.

Ru(II) Complexes as PDT Agents. PDT is a noninvasive means of treating cancer, whereby an otherwise nontoxic photosensitizer (PS) is activated by light to destroy tumors and tumor vasculature.[35,36] Although not widely recognized, PDT is also capable of initiating potent immune responses, including innate and adaptive antitumor immunity. The advantage of PDT over mainstream forms of cancer therapy is that it is highly selective, with toxicity confined to regions where PS, oxygen, and light overlap in space and time. Off-site toxicity is thus minimized by selective illumination of only malignant tissue. Traditionally, PDT has relied on organic PSs that generate cytotoxic singlet oxygen ($^1O_2$) from triplet excited states. This reliance on $^1O_2$ for cytotoxic effects is a salient drawback and significantly diminishes the PDT effect in hypoxic tissue and solid tumors. In addition, the organic PSs approved for clinical use cannot be activated by wavelengths of light that penetrate tissue best (e.g., >700 nm), limiting their use to superficial lesions. These and other limitations associated with organic, porphyrin-based PSs have sparked an interest in the use of metal complexes as PSs for PDT.[37]

Ru(II) complexes have received much attention for this purpose owing to well-characterized excited states that can be tuned rationally with straightforward synthetic manipulations. For example, introduction of one or more strained ligands in tris-bidentate constructs lowers the energy of dissociative metal-centered (MC) excited states that can exert oxygen-independent phototoxic effects by covalent modification of biomolecules such as DNA.[38] π-Expansive ligands lower the energy of ligand-centered (LC) excited states that have extremely long intrinsic lifetimes, making the systems very sensitive to oxygen and able to form cytotoxic $^1O_2$ at low oxygen tension.[22,39] Some of these π-expansive ligands participate in excited-state redox reactions in the absence of oxygen, making them excellent PSs for PDT in hypoxia. This ability to switch between photocytotoxic mechanisms as a function of oxygen tension is a key feature of some of the most promising Ru(II) complexes developed to date, with some Ru(II) complexes able to sensitize phototoxic reactions even with wavelengths of light where absorption is minimal (<100 M^{-1} cm^{-1}).[39b]

One exemplary π-expansive ligand that we and others[39a,b] have employed previously is benzo[*i*]dipyrido[3,2-*a*:2′,3′-*c*]-phenazine (dppn) (structure shown in Chart 1). [Ru-

Chart 1. Molecular Structures of the Ru(II) Complexes 1−5

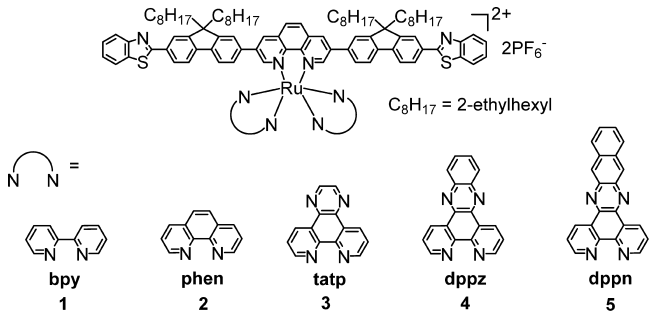

$(bpy)_2dppn]^{2+}$ was shown to be a powerful phototoxic agent in vitro with no dark cytotoxicity, to function in the absence of oxygen, to have excellent water and saline solubility, and to be activated effectively by 625 nm light. Its near-unity quantum yield for triplet state formation and long intrinsic excited-state lifetime (33 μs)[39a] make $[Ru(bpy)_2dppn]^{2+}$ an excellent model Ru(II) complex not only for PDT applications but also for RSA.

In the present work, we combined the ligands that showed favorable properties for each application into a single construct (Chart 1) with the goal of establishing structure−property relationships for RSA and in vitro PDT in heteroleptic tris-diimine Ru(II) complexes. The benzothiazolylfluorenyl (BTF)-substituted phenanthroline ligand (**L**) was chosen based on its demonstrated utility when incorporated into Ir(III) scaffold, which exhibited broad and intense excited-state absorption in the visible to the NIR region, a long triplet lifetime (13 μs), and intense RSA at 532 nm for nanosecond laser pulses.[40] Selection of bpy, phen, tatp, dppz, or dppn as the set of coligands was based on the results by Chao and Ji, whose work demonstrated that the extended π-conjugation of these ligands systematically increased the third-order susceptibility of the $[Ru(PIP)_2(N^N)](ClO_4)_2$ complexes,[27] and on our study of the corresponding $[Ru(bpy)_2(N^N)]^{2+}$ series, where N^N = phen, tatp, dppz, or dppn, which showed an identical trend for in vitro PDT potency.[39b]

DOI: 10.1021/acs.inorgchem.6b02624
Inorg. Chem. 2017, 56, 3245−3259

Scheme 1. Synthetic Route[a] for Complexes 1−5

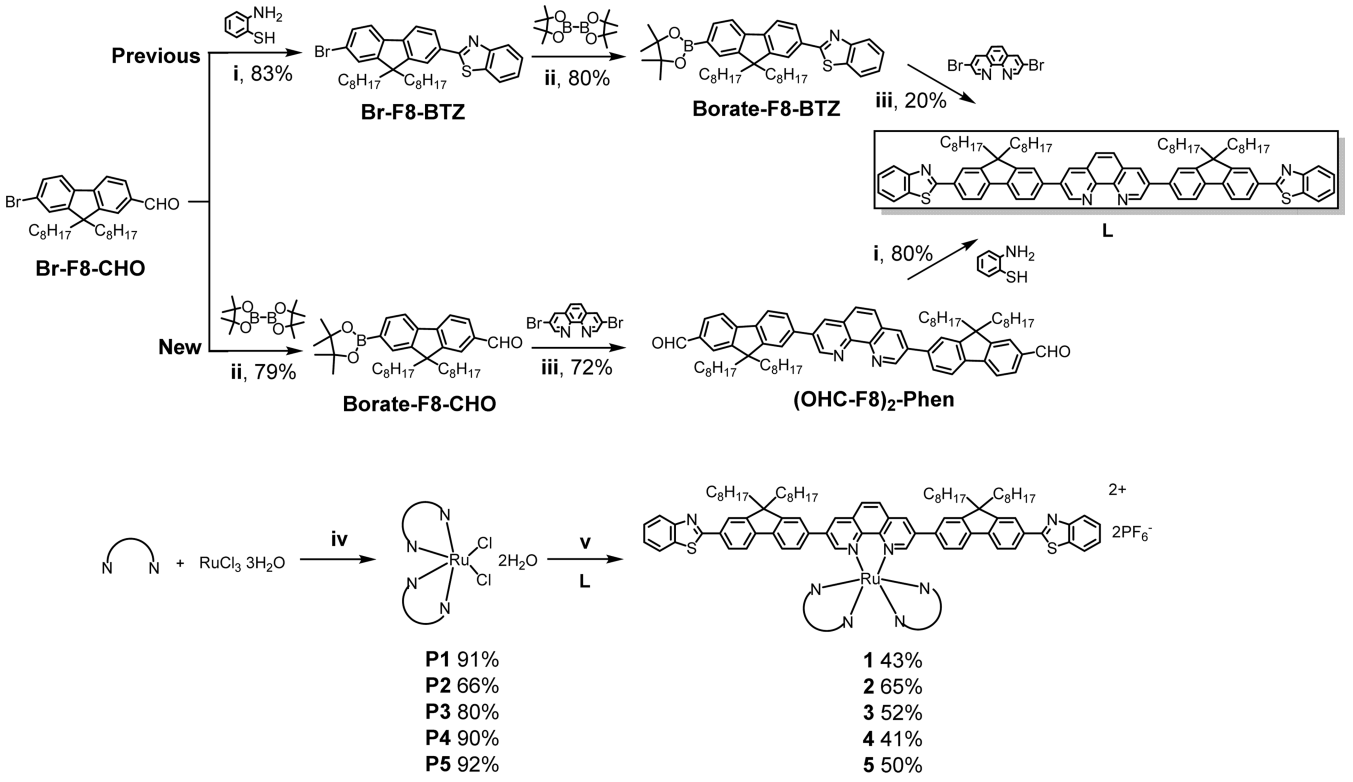

[a](i) DMSO, reflux 90 min; (ii) $Pd(dppf)Cl_2$, KOAc, dioxane, 80 °C; (iii) $Pd(PPh_3)_4$, K_2CO_3, toluene/H_2O, 110 °C; (iv) LiCl, DMF, reflux 24 h; (v) EtOH, reflux, 24 h (**1**, **2**) or ethylene glycol, reflux 5 h (**3**, **4**, **5**).

EXPERIMENTAL SECTION

Synthesis and Characterization. All reagents and solvents were purchased from commercial sources and used as is unless otherwise mentioned. ^1H NMR spectra were recorded on a Varian Oxford-400/Bruker-400 spectrometer in $CDCl_3$ with tetramethylsilane ($Si(CH_3)_4$) as the internal standard. High-resolution mass spectrometry (HRMS) analyses were performed on Waters Synapt G2-Si Mass Spectrometer. Elemental analyses were conducted by NuMega Resonance Laboratories, Inc. in San Diego, California. The BTF-substituted 1,10-phenanthroline ligand **L** (structure shown in Scheme 1) was synthesized using a modified procedure from our previously reported method.[40a] The ancillary diimine ligand (N^N) 1,4,8,9-tetra-azatriphenylene (tatp), dipyrido[3,2-*a*:2′,3′-*c*]phenazine (dppz), benzo[*i*]dipyrido[3,2-*a*:2′,3′-*c*]phenazine (dppn),[41] and the corresponding ruthenium precursor *cis*-$(N^N)_2RuCl_2$[42] were synthesized according to the literature procedures.

Borate-F8-CHO. In the absence of light, a mixture of 7-bromofluorene-2-carbaldehyde (**Br−F8−CHO**)[43] (2.44 g, 4.9 mmol), 4,4,4′,4′,5,5,5′,5′-octamethyl-2,2′-bi-1,3,2-dioxaborolane (1.49 g, 5.8 mmol), $Pd(dppf)Cl_2{\cdot}CH_2Cl_2$ (108 mg, 0.14 mmol), KOAc (1.5 g, 15 mmol), and dioxane (30 mL) was stirred at 80 °C for 24 h. After the reaction mixture was cooled to room temperature (rt), ethyl acetate (50 mL) was added. The organic layer was separated and washed with brine and dried over anhydrous $MgSO_4$. After removal of the solvent, the crude product was purified by column chromatography (silica gel, hexane/ethyl acetate (40:1, v/v)) to afford **Borate-F8-CHO** as pale yellow oil (2.1 g, yield: 79%). ^1H NMR (400 MHz, $CDCl_3$): δ 10.05 (s, 1H), 7.90−7.86 (m, 4H), 7.84−7.82 (d, J = 8.0 Hz, 1H), 7.78−7.76 (d, J = 8.0 Hz, 1H), 2.08−2.00 (m, 4H), 1.37 (s, 12H), 0.77−0.65 (m, 24H), 0.50−0.41 (m, 6H).

(OHC-F8)$_2$-Phen. Compounds **Borate-F8-CHO** (720 mg, 1.32 mmol) and 3,8-dibromophenanthroline (203 mg, 0.60 mmol) were mixed in a 100 mL Schlenk tube. Then $Pd(PPh_3)_4$ (200 mg, 0.17 mmol) and K_2CO_3 (547 mg, 4.0 mmol) were added. The reaction system was vacuumed and backfilled with argon three times. After that, degassed toluene (10 mL) and water (5 mL) were added as the solvent. The mixture was heated to 110 °C for 48 h in the absence of light. After the reaction mixture was cooled to rt, it was poured into water and extracted with CH_2Cl_2. The CH_2Cl_2 layer was dried over $MgSO_4$, and then the solvent was removed in vacuum. The residue was purified by column chromatography (silica gel, hexane/ethyl acetate (30:1, v/v)) to afford the product as yellow oil (430 mg, yield: 72%). ^1H NMR (400 MHz, $CDCl_3$): δ 10.09 (s, 2H), 9.50 (s, 2H), 8.45 (t, J = 4.0 Hz, 2H), 7.98−7.93 (m, 10H), 7.84−7.82 (m, 4H), 2.15 (m, 8H), 0.87−0.80 (m, 32 H), 0.66−0.49 (m, 28H). Electrospray ionization (ESI)-HRMS calcd. for $[C_{72}H_{88}N_2O_2]^+$: 1013.6924; Found: 1013.6910.

*Ligand **L**.* The mixture of **(OHC-F8)$_2$-Phen** (430 mg, 0.43 mmol), 2-aminothiophenol (0.11 mL, 1.1 mmol), and dimethyl sulfoxide (DMSO; 15 mL) was stirred at 195 °C under argon for 90 min. The reaction mixture was allowed to cool to rt and poured into 100 mL of water. After extraction with ethyl acetate, the combined organic layer was dried over $MgSO_4$. Then the solvent was removed, and the crude product was purified by column chromatography (silica gel, hexane/ethyl acetate (5:1, v/v)) to afford **L** as pale yellow solid (420 mg, 80%). ^1H NMR (400 MHz, $CDCl_3$): δ 9.49 (s, 2H), 8.43 (t, J = 4.0 Hz, 2H), 8.19−8.08 (m, 6H), 7.94−7.86 (m, 8H), 7.81−7.79 (m, 4H), 7.52 (t, J = 8.0 Hz, 2H), 7.40 (t, J = 8.0 Hz, 2H), 2.21−2.17 (m, 8H), 0.91−0.84 (m, 32H), 0.65−0.53 (m, 28H). ESI-HRMS calcd. for $[C_{84}H_{94}N_4S_2]^+$: 1223.6998; Found: 1223.6995.

*General Procedure for the Synthesis of Complexes **1** and **2**.* Compounds *cis*-$(N^N)_2RuCl_2$ (0.05 mmol) and **L** (61.2 mg, 0.05 mmol) and 20 mL of ethanol were added to a 50 mL round-bottom flask. The reaction mixture was vacuumed and backfilled with argon three times and then heated to reflux for 24 h. After the reaction mixture was cooled to rt, 80 mg NH_4PF_6 was added and then stirred at rt for 2 h. The solvent was removed under vacuum, and then the crude product was purified by column chromatography (silica gel, 60 Å).

*Complex **1**.* CH_2Cl_2/CH_3OH (80:1, v/v) was used as the eluent, and the product was obtained as a red-orange solid (45 mg, yield:

DOI: 10.1021/acs.inorgchem.6b02624
Inorg. Chem. 2017, 56, 3245−3259

43%). ^{1}H NMR (400 MHz, $CDCl_3$): δ 8.60 (s, 2H), 8.40−8.36 (m, 4H), 8.23−8.20 (m, 4H), 8.11−7.96 (m, 12H), 7.88 (m, 4H), 7.81−7.72 (m, 4H), 7.58−7.50 (m, 6H), 7.49−7.43 (m, 4H), 7.37 (t, J = 8.0 Hz, 2H), 2.15−2.02 (m, 8H), 0.81−0.30 (m, 60H). ESI-HRMS calcd. for $[C_{104}H_{110}RuN_8S_2]^{2+}$: 818.3683; Found: 818.3637. Anal. calcd. (%) for $C_{104}H_{110}F_{12}N_8P_2RuS_2{\cdot}3H_2O{\cdot}0.5C_7H_{16}$: C, 63.56; H, 6.15; N, 5.52. Found: C, 63.39; H, 6.53; N 5.91.

Complex **2**. CH_2Cl_2/CH_3OH (50:1, v/v) was used as the eluent, and the obtained product was washed with heptane to afford the final prodcut as a red solid (65 mg, yield: 65%). ^{1}H NMR (400 MHz, $CDCl_3$): δ 8.56 (s, 2H), 8.41−8.33 (m, 8H), 8.25−8.21 (m, 2H), 8.13−8.07 (m, 12H), 7.93−7.79 (m, 10H), 7.65−7.58 (m, 2H), 7.52−7.37 (m, 6H), 2.13−1.97 (m, 8H), 0.88−0.38 (m, 56 H), −0.02 to −0.04 (m, 4H). ESI-HRMS calcd. for $[C_{108}H_{110}RuN_8S_2]^{2+}$: 842.3683; Found: 842.3641. Anal. calcd. (%) for $C_{108}H_{110}F_{12}N_8P_2RuS_2{\cdot}3H_2O{\cdot}C_7H_{16}$: C, 64.80; H, 6.34; N, 5.26. Found: C, 64.96; H, 6.61; N 5.57.

General Procedure for the Synthesis of Complexes **3**−**5**. Compounds *cis*-$(N^N)_2RuCl_2$ (0.05 mmol) and **L** (61.2 mg, 0.05 mmol), and 20 mL of ethylene glycol were added to a 50 mL round-bottom flask. The reaction mixture was bubbled with argon for 30 min and then heated to reflux for 5 h. After the reaction mixture was cooled to room temperature, 80 mg of NH_4PF_6 was added, and the mixture was stirred at room temperature for 2 h. After that, water was added, and the mixture was extracted by CH_2Cl_2. The CH_2Cl_2 layer was dried over $MgSO_4$, and then the solvent was removed. The residue solid was purified by column chromatography (silica gel, 60 Å) to afford the final product.

Complex **3**. CH_2Cl_2/CH_3OH (60:1, v/v) was used as the eluent, and the obtained product was washed with hexane to afford red solid as the final product (52 mg, yield: 52%). ^{1}H NMR (400 MHz, $CDCl_3$): δ 9.59−9.56 (m, 4H), 9.15−9.13 (m, 4H), 8.63−8.62 (m, 4H), 8.48−8.42 (m, 2H), 8.32−8.28 (m, 4H), 8.14−8.02 (m, 10H), 7.93 (d, J = 8.0 Hz, 2H), 7.86−7.79 (m, 4H), 7.70 (m, 2H), 7.54−7.50 (m, 2H),7.43−7.35 (m, 4H), 2.10−1.92 (m, 8H), 0.91−0.15 (m, 56H), −0.03 to −0.05 (m, 4H). ESI-HRMS calcd. for $[C_{112}H_{110}RuN_{12}S_2]^{2+}$: 894.3745; Found: 894.3708. Anal. calcd (%) for $C_{112}H_{110}F_{12}N_{12}P_2RuS_2$: C, 64.70; H, 5.33; N, 8.08. Found: C, 64.59; H, 5.70; N 7.72.

Complex **4**. CH_2Cl_2/CH_3OH (60:1, v/v) was used as the eluent, and the obtained product was washed with hexane to afford brown solid as the final product (45 mg, yield: 41%). ^{1}H NMR (400 MHz, $CDCl_3$): δ 9.71 (m, 4H), 8.67−8.65 (m, 4H), 8.43−8.40 (m, 10H), 8.11−7.77 (m, 22H), 7.54−7.50 (m, 2H), 7.45−7.36 (m, 4H), 2.01−1.84 (m, 8H), 0.84−0.27 (m, 56H), 0 to −0.03 (m, 4H). ESI-HRMS calcd. for $[C_{120}H_{114}RuN_{12}S_2]^{2+}$: 944.3903; Found: 944.3860. Anal. calcd. (%) for $C_{120}H_{114}F_{12}N_{12}P_2RuS_2{\cdot}0.5C_7H_{16}$: C, 66.53; H, 5.52; N, 7.54. Found: C, 66.41; H, 5.70; N 7.43.

Complex **5**. CH_2Cl_2/CH_3OH (60:1, v/v) was used as the eluent, and the obtained product was wahsed with hexane to afford brown solid as the final product (75 mg, yield: 50%). ^{1}H NMR (400 MHz, $CDCl_3$): δ 9.56 (m, 4H), 9.08−8.90 (m, 4H), 8.57 (m, 4H), 8.51 (m, 2H), 8.33−7.73 (m, 28H), 7.55−7.40 (m, 8H), 2.32−1.82 (m, 8H), 0.94−0.30 (m, 56H), 0 to −0.1 (m, 4H). ESI-HRMS calcd. for $[C_{128}H_{118}RuN_{12}S_2]^{2+}$: 994.4060; Found: 994.4016. Anal. calcd. (%) for $C_{128}H_{118}F_{12}N_{12}P_2RuS_2$: C, 67.44; H, 5.22; N, 7.37. Found: C, 67.26; H, 5.53; N 7.17.

Photophysical Measurements. The solvents (spectroscopic grade) used for photophysical studies were purchased from VWR International and used without further purification. The ultraviolet−visible (UV−vis) absorption spectra were recorded on a Varian Cary 50 spectrophotometer. Steady-state emission spectra were obtained on a Jobin-Yvon FluoroMax-4 fluorometer/phosphorometer. The emission quantum yields were determined by the relative actinometry method in degassed solvent, in which $[Ru(bpy)_3]Cl_2$ in degassed CH_3CN (λ_{max} = 436 nm, Φ_{em} = 0.097)[44] was used as reference for all of the complexes.

The nanosecond transient difference absorption (TA) spectra and decays were measured in degassed CH_3CN solutions on an Edinburgh LP920 laser flash photolysis spectrometer. The third harmonic output (355 nm) of a Nd:YAG laser (Quantel Brilliant, pulse width = 4.1 ns; the repetition rate was set to 1 Hz) was used as the excitation source. Each sample was purged with argon for 45 min prior to measurement. The triplet excited-state absorption coefficient (ε_T) at the TA band maximum was determined by the singlet depletion method.[45] The triplet quantum yield was obtained using the relative actinometry method[46] using SiNc in benzene ($\varepsilon_{590\ nm}$ = 70 000 L mol^{-1} cm^{-1}, Φ_T = 0.20) as the reference.[47]

Computational Methods. The details of the computational methods for ground-state and excited-state geometry optimization of **1**−**5**, and simulation of their electronic absorption spectra and calculation of their emission energies, are provided in the Supporting Information. The experimental details of cell culture, cytotoxicity and photocytotoxicity, DNA photocleavage assays, and confocal microscopy studies are provided in the Supporting Information.

RESULT AND DISCUSSION

Synthesis. Scheme 1 shows the synthetic route for complexes **1**−**5**. The Ru(II) precursors *cis*-$(N^N)_2RuCl_2$ (N^N = bpy, phen, tatp, dppz, dppn) were prepared following the methods described for the synthesis of *cis*-$(bpy)_2RuCl_2$, in which 2 equiv of N^N ligands were mixed with $RuCl_3{\cdot}3H_2O$ in anhydrous dimethylformamide (DMF) and then refluxed for 24 h.[42] During this procedure, Ru(III) was reduced to Ru(II) by the volatile dimethylamine generated in situ by decomposition of DMF at its boiling temparature followed by coordination of ligands to the metal.[48] The desired products were precipitated by adding acetone to the reaction mixture, and the solid collected was used directly in the next reaction without further purification.

The ligand **L** was syntheized by modification of the procedure previously reported by us,[40a] where we performed the cyclization reaction of 7-bromofluorene-2-carbaldehyde (**Br−F8−CHO**) with 2-aminothiophenol, to obtain **Br−F8−BTZ** first, and then converted **Br−F8−BTZ** to **Borate-F8-BTZ**. **Borate-F8-BTZ** was then coupled with 3,8-dibromo-1,10-phenanthroline to give ligand **L**. The low yield (20%) of the Suzuki coupling reaction was due to the formation of both the desired bisubstituted product and the undesired monosubstituted byproduct, which was proven to be difficult to separate from the bisubstituted product. To aid separation and improve yields, the reaction sequence was altered by converting **Br−F8−CHO** to **Borate-F8-CHO** first and then performing the Suzuki coupling reaction to obtain **(OHC-F8)$_2$-Phen**. Almost no monosubstituted byproduct was detected after the reaction, increasing the yield to 72% for the desired bisubstituted product. Cyclization of **(OHC-F8)$_2$-Phen** afforded **L** in 80% yield. This resulted in an overall yield of 46% for the three steps starting from **Br−F8−CHO**, which is more than 3 times higher than the previous overall yield (13%). The final Ru(II) complexes were synthesized by refluxing the Ru(II) precursors *cis*-$(N^N)_2RuCl_2$ with 1 equiv of **L** in either ethanol (for **1** and **2**) or ethylene glycol (for **3**−**5**) based on the solubility of the Ru(II) precursors. All complexes were purified by column chromatography on silica gel, and the structures were verified by ^{1}H NMR, HRMS, and elemental analysis. The complexes showed good solubility in CH_2Cl_2, $CHCl_3$, CH_3CN, and DMSO and were quite stable even in coordinating solvents such as CH_3CN and DMSO (monitored by thin-layer chromatography (TLC) for the sample solutions in air at rt for at least two weeks). It is worth noting that except for complex **1**, the ^{1}H NMR spectra of the other four complexes all contain multiplets with chemical shifts less than 0. As the π-conjugation of the ancillary N^N ligands increases, these multiplets become broader.

DOI: 10.1021/acs.inorgchem.6b02624
Inorg. Chem. 2017, 56, 3245−3259

Electronic Absorption. The UV−vis absorption spectra of complexes **1**−**5** were measured in CH_2Cl_2 and are compared to the calculated absorption spectra in Figure 1 (see also Figures S1 and S2 in Supporting Information). The absorption band maxima and molar extinction coefficients are compiled in Table 1.

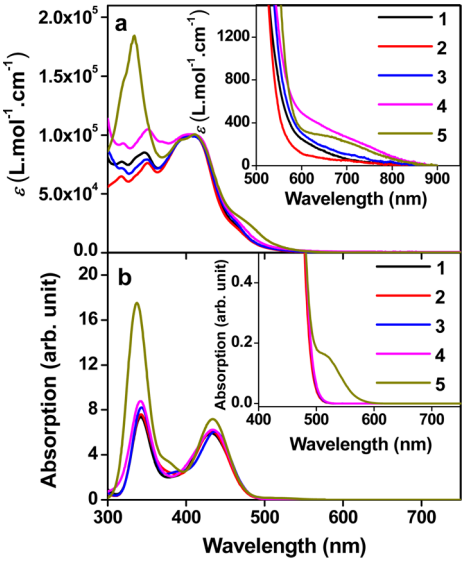

Figure 1. Experimental and calculated absorption spectra of complexes **1**−**5** in CH_2Cl_2. (a) Experimental absorption spectra. (inset) Expansion of the spectra between 500 and 900 nm. (b) The calculated absorption spectra using PBE1PBE.

The spectra of **1**−**5** all consist of intense absorption bands at wavelengths shorter than 350 nm and a broad, featureless band at near 410 nm. The structured features and large molar extinction coefficients (7×10^4 to 1.8×10^5 M^{-1} cm^{-1}, Table 1) for the bands below 350 nm were consistent with the $^1\pi,\pi^*$ nature of the transitions. This assignment is supported by the excited orbitals, the natural transition orbitals (NTOs),[49] obtained from the time-dependent density functional theory (TDDFT) calculations (Supporting Information Table S1). For all complexes, the NTOs revealed predominant contributions from the $^1\pi,\pi^*$ transition based on the **L** ligand, with nominal intraligand charge transfer (^{1}ILCT) and metal-to-ligand charge transfer (^{1}MLCT) character. However, complex **5** showed a significant contribution from the ^{1}ILCT transition within the dppn ligand, which markedly enhanced the intensity of the band centered near 335 nm.

The featureless band near 410 nm ($\varepsilon = 1 \times 10^5$ M^{-1} cm^{-1}) remained at constant energy and intensity for all complexes, independent of the ancillary ligands. This implies that the nature of the transitions contributing to this band is likely the same and that the transitions should originate from the same structural component, that is, the **L** ligand. The structureless feature suggests a charge-transfer nature for this band, but the intensity of this band indicates $^1\pi,\pi^*$ contribution. The NTOs corresponding to the transitions at ca. 440 nm (shown in Supporting Information Table S2) clearly manifest the major contributing transitions being the ^{1}ILCT/$^1\pi,\pi^*$ transitions localized on the **L** ligand, admixed with some ^{1}MLCT character. Note that in the experimental spectra, the ^{1}MLCT transition exhibited some degree of separation from the ^{1}ILCT/$^1\pi,\pi^*$ transitions, as reflected by the shoulder near 470 nm for all complexes. However, in the calculated spectra, these transitions merged into one band. For complex **5**, the shoulder at 470 nm is more salient. As predicted by the calculation, an absorption band at 517 nm with $^1\pi,\pi^*$ character associated with the dppn ancillary ligands should be observed. Considering the fact that the calculated spectra are somewhat red-shifted compared to the experimental spectra, we attribute the more pronounced shoulder in **5** to the additional contribution from the dppn ligand $^1\pi,\pi^*$ transition.

In addition to these major absorption bands, studies on concentrated solutions (5×10^{-5} to 2×10^{-4} M) revealed a broad but very weak absorption band (ε < 800 M^{-1} cm^{-1}) in the spectral range of 550−900 nm (see inset in Figure 1a), which is more pronounced in **4** and **5**. Considering the very small molar extinction coefficients, we assign these transitions as direct spin-forbidden population of triplet excited states due to the strong spin−orbit coupling in these complexes. Such a weak but broad absorption band in the visible to the NIR region is a desirable feature for developing broadband reverse saturable absorbers and PDT agents. Increasing the π-conjugation of the ancillary ligands mainly influenced the nature of the lowest-energy singlet and triplet transitions.

The UV−vis absorption spectra of complexes **1**−**5** showed very minor solvatochromic effects (Supporting Information Figure S3) in solvents used in this study (CH_3CN, CH_2Cl_2, and toluene) as would be expected for transition-metal complexes with a pseudo-octahedral configuration, which prevents the solvent molecules from approaching the Ru(II) ion.

Table 1. Photophysical Data for Complexes 1−5

	λ_{abs},[a] nm (ε/1 × 10^4 M^{-1} cm^{-1})	λ_{em},[b] nm (τ, μs); Φ_{em} rt	λ_{em},[c] nm 77 K	$\lambda_{T1\text{-}Tn}$, nm (τ_T, μs; $\varepsilon_{T1\text{-}Tn}$, 1 × 10^4 M^{-1} cm^{-1}); Φ_T[d]
1	289 (10.7), 318 (7.8), 346 (8.5), 406 (10.0), 470 (1.9)	603 (1.25), 640 (1.32); 0.063	594, 644	507 (1.83; 3.03), 717 (1.80; 2.94); 0.37
2	317 (6.5), 351 (7.6), 405 (10.0), 467 (1.9)	600 (0.88), 640 (0.89); 0.050	589, 636	504 (2.03; 2.92), 717 (1.91; 2.57); 0.38
3	298 (8.7), 319 (7.2), 350 (7.9), 407 (9.9), 467 (2.3)	595 (0.43), 650 (0.42); 0.056	581, 629	444 (0.89; 1.16), 501 (0.84; 2.52), 720 (0.85; 2.63); 0.37
4	286 (14.6), 320 (9.3), 351 (10.4), 407 (10.1), 470 (2.3), 680 (0.02, br)	597 (0.59), 640 (0.59); 0.049	581, 637	441 (0.96; 2.64), 510 (1.08; 1.83), 705 (1.11; 2.44); 0.17
5	334 (18.4), 391 (9.5, sh), 410 (10.1), 470 (2.9), 700 (0.02, br)	557 (0.02), 601 (0.02), 646 (0.02) ; 0.005	594, 646	543 (41.2; -); -

[a]Absorption band maxima and molar extinction coefficients in CH_2Cl_2 at rt. [b]The rt emission band maxima, lifetimes, and emission quantum yields measured in CH_2Cl_2. A degassed $[Ru(bpy)_3]Cl_2$ CH_3CN solution was used as the reference (Φ_{em} = 0.097, λ_{ex} = 436 nm). [c]Emission band maxima in butyronitrile glassy matrix at 77 K. [d]Nanosecond transient absorption band maxima, triplet extinction coefficients, triplet excited-state lifetimes, and quantum yields measured in CH_3CN at rt. SiNc in benzene was used as the reference ($\varepsilon_{590\ nm}$ = 70 000 L mol^{-1} cm^{-1}, Φ_{em} = 0.20).[47]

DOI: 10.1021/acs.inorgchem.6b02624
Inorg. Chem. 2017, 56, 3245−3259

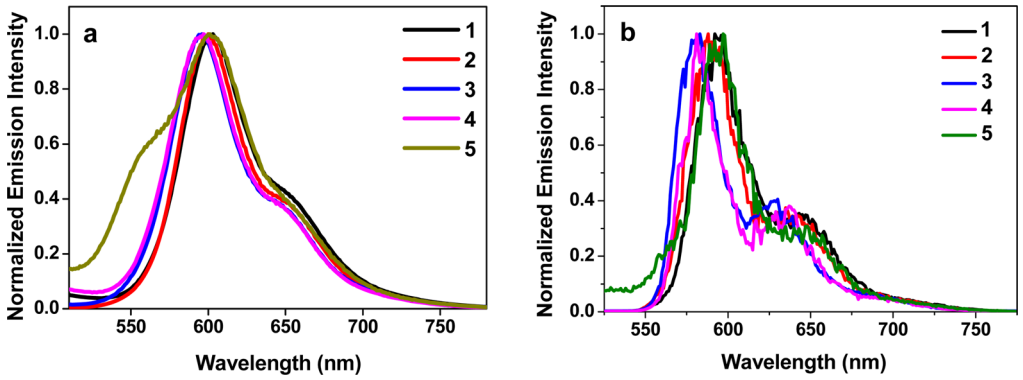

Figure 2. Normalized emission spectra of complexes **1** (λ_{ex} = 405 nm), **2** (λ_{ex} = 405 nm), **3** (λ_{ex} = 405 nm), **4** (λ_{ex} = 403 nm), and **5** (λ_{ex} = 413 nm) in deaerated CH_2Cl_2 at rt (a) and in glassy butyronitrile matrix at 77 K (b).

Photoluminescence. Complexes **1**−**5** all exhibited red-orange luminescence at rt in deaerated solution and in glassy matrix at 77 K. The normalized emission spectra of **1**−**5** in CH_2Cl_2 at rt and in butyronitrile glassy matrix at 77 K are shown in Figure 2, and the emission quantum yields and lifetimes at rt are provided in Table 1. Because the emission spectra are somewhat structured even at rt, the emission lifetimes were measured at the band maximum and the shoulder(s) to ensure that they originate from the same excited state. The emission from complexes **1**−**5** was significantly red-shifted with respect to their corresponding excitation wavelengths, and their emission lifetimes varied from tens of nanoseconds to 1.3 μs. Thus, we assign the observed emission to phosphorescence. The polarity and nature of the solvent (coordinating vs noncoordinating) had only minor effects on the emission energies of these complexes (see Supporting Information Figure S4), but the emission lifetimes and quantum yields of **1**−**4** were increased in CH_3CN and toluene in comparison to those in CH_2Cl_2. This solvent dependence was not observed for **5** (see Supporting Information Table S3).

It is worth noting that, unlike the reported $[Ru(bpy)(dppn)_2]^{2+}$ complex that is not emissive in CH_3CN or H_2O,[50] complex **5** with the similar core ligands but with π-conjugated BTF substituents on bpy is weakly emissive in all of the solvents used (i.e., CH_2Cl_2, CH_3CN, and toluene). The possibility of the observed emission of **5** being from a trace amount of impurity (ligand **L** or $Ru(dppn)_2Cl_2$ precursor) has been ruled out based on these facts: (1) the TLC test of **5** did not show any additional detectable emissive spots; (2) the excitation spectra monitored at the emission band maximum and shoulders (see Supporting Information Figure S5) were all the same and resembled the UV−vis absorption spectrum of **5**; (3) ligand **L** emitted in the blue region (λ_{max} = 416 nm), and $Ru(dppn)_2Cl_2$ emitted at 569 nm (which is 32 nm blue-shifted compared to the emission band maximum of **5** at 601 nm) with longer lifetime (80 ns for $Ru(dppn)_2Cl_2$ vs 20 ns for **5**). Therefore, the observed emission cannot be from either of them.

The emission energies of **1**−**5** were essentially independent of the ancillary ligand identities, implying that the emission of these complexes could originate from the same structural component, namely, the **L** ligand. The vibronic progression of 1200−1420 cm^{-1} was typical of $^3\pi,\pi^*$ states. Because the emission lifetimes were much shorter than what is usually observed for $^3\pi,\pi^*$ emitting states and similar to what would be expected for ^{3}CT (CT = charge transfer) states, the emitting state should have some ^{3}CT character. Therefore, the emitting states of **1**−**5** are tentatively assigned as the $^3\pi,\pi^*/^3$CT states.

Such assignments are supported by the TDDFT calculations. Although the calculated phosphorescence energies (~737 nm) appeared to be underestimated compared to the experimental results, which is a common challenge for simulating the triplet excited states with charge transfer character using TDDFT,[51] the trend of the calculated phosphorescence energies reproduced the trend of the experimental results very well. This approach has also been demonstrated to provide reasonable qualitative properties of excited states in many other molecules, including Ir(III) complexes.[51b] More importantly, the obtained NTOs can aid in our understanding of the nature of the emitting states in **1**−**5**. As the NTOs in Supporting Information Table S4 indicated, the holes of **1**−**4** are predominantly distributed on one of the BTF components of the **L** ligand, with minor contribution from the Ru(II) d orbital, while the electrons are on the same BTF motif but delocalized to the phenanthroline unit. Therefore, the nature of the lowest triplet state (T_1) for **1**−**4** has $^3\pi,\pi^*/^3$MLCT/^{3}ILCT character. In contrast, the calculations showed that the T_1 state of **5** was dppn-localized $^3\pi,\pi^*$ state, with an underestimated calculated energy compared to the experimental emission energy of **5** (T_1^{theo} = 957 nm vs T^{exp} = 601 nm). However, the calculated T_3 state energy of **5** is at nearly the same energy and with the similar $^3\pi,\pi^*/^3$MLCT/^{3}ILCT character as those of complexes **1**−**4**, which is in better agreement with the experimental emission energy as well. It has been reported that other Ru(II) complexes containing the dppn ligand emit from a high-lying ^{3}MLCT excited state rather than the lowest dppn $^3\pi,\pi^*$ state (T_1 state).[39a,52] This also appeared to be the case for complex **5**, with the emission originating from the high-lying T_3 state. Such a high-lying emitting state also accounts for the much shorter emission lifetime of complex **5** (0.02 μs) compared to those of the other four complexes (0.4−1.2 μs, see Table 1) although the nature of the emitting state is the same. Thus, we conclude that the emission of all complexes has mixed $^3\pi,\pi^*/^3$MLCT/^{3}ILCT character associated with the **L** ligand. The difference between **1**−**4** and **5** lies in whether the emitting state is T_1 or T_3 (for **5** it is T_3).

The emission measurements at 77 K also supported the $^3\pi,\pi^*/^3$CT nature of the emitting states. As shown in Figure 2b, the emission spectra of **1**−**5** became narrower and more structured. Meanwhile, they were slightly blue-shifted (see comparison of the emission spectra at rt and at 77 K in BuCN in Supporting Information Figure S6) due to the rigidochromic

DOI: 10.1021/acs.inorgchem.6b02624
Inorg. Chem. 2017, 56, 3245−3259

effect.[53] The thermally induced Stokes shifts were in the range of 330−550 cm^{-1}, which are consistent with the predominant $^3\pi,\pi^*$ nature of the emitting states.

Although the emission energies and nature of the emitting states for **1**−**5** are quite similar, fusion of the pyrazine ring to the phenanthroline ligand caused a slight blue shift of the emission spectrum of **3** compared to that of **2**. However, benzannulation on tatp (the ancillary ligands in **3**) induced a minor red shift of the emission spectra of **4** and **5**, which is possibly due to the increased π-conjugation of the ancillary ligands. Nevertheless, the emission lifetimes of **3**−**5** are noticeably shorter than those of **1** and **2**.

The emission lifetimes of all of the complexes at different concentrations (5×10^{-6} to 1×10^{-4} M) at rt were also investigated. We found that the lifetimes remained almost constant in the concentration range studied, indicating the absence of self-quenching in these complexes. This is most reasonably attributed to the presence of the branched alkyl chains on the **L** ligand, which prevents any significant intermolecular interactions of these complexes in solutions.

Transient Absorption. Nanosecond transient absorption (TA) measuremens not only provide information on the excited-state absorption spectrum but also afford the triplet excited-state decay time and the triplet excited-state quantum yield. Because RSA is closely related to the excited-state absorption, studying the TA characteristics of **1**−**5** enables us to assess the spectral range where RSA could occur. The TA spectra of **1**−**5** in deaerated acetonitrile solutions at zero-time delay recorded upon excitation at 355 nm at rt are shown in Figure 3 (the time-resolved nanosecond TA spectra of **1**−**5** are provided in Supporting Information Figure S7). The TA band maxima and the excited-state molar extinction coefficients, the excited-state lifetimes deduced from the decay of the TA, and the triplet quantum yields obtained from actinometry for these complexes are listed in Table 1.

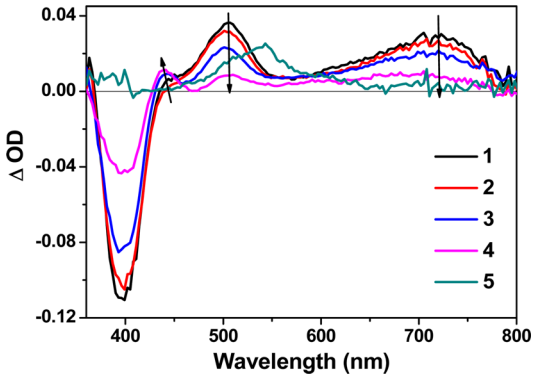

Figure 3. Triplet TA spectra of complexes **1**−**5** in acetonitrile solution (λ_{ex} = 355 nm, A_{355} = 0.4 in a 1 cm cuvette) at zero-time delay.

The TA spectra of all complexes featured broad positive absorption band(s) from 430 to 800 nm. With the exception of complex **5**, the spectra of **1**−**4** were similar in shape with two major absorption bands near 500 and 710 nm and a shoulder at ∼440 nm. However, the relative intensities of the 500 and 710 nm bands gradually decreased from **1** to **4**, while the intensity of the 440 nm shoulder slightly increased and was blue-shifted on going from **1** to **4**. In addition, **1**−**4** exhibited a ground-state bleach centered at 400 nm, due to their respective ^{1}ILCT/$^1\pi,\pi^*$ transitions. Considering the similar TA spectral features and the similar TA and emission lifetimes for complexes **1**−**4** in CH_3CN (Supporting Information Table S3), we attribute the observed TA to the ^{3}ILCT/$^3\pi,\pi^*$ states associated with the **L** ligand. This assignment was supported by (i) the similarity of the TA spectrum of **1** to that of its corresponding biscyclometalated Ir(III) complex with the same **L** ligand[40a] and (ii) the similarities in the energies and shapes of the 500 and 710 nm bands to those of **L** coordinated to Zn^{2+} (see Supporting Information Figure S8), which has the transient absorbing ^{3}ILCT/$^3\pi,\pi^*$ states. Changing the ancillary ligand from bpy to phen produced only minor effects on the TA characteristics of complexes **1** and **2** (except for the slightly decreased intensity of the two bands in complex **2**), while fusing the pyrazine ring to the phen ligands induced a new band near 440 nm for **3**. The intensity of this band further increased with extension of the π-conjugation of the ancillary ligands via benzannulation as in complex **4**. However, the two absorption bands at 500 and 710 nm decreased in **3** and **4**. Assuming a similar origin of the transient absorbing species for complexes **1**−**4**, the attenuated intensity of these two major TA bands was ascribed to the gradual increase of the ground-state absorption from 450 to 800 nm.

The TA feature of **5** is dramatically different from those of **1**−**4**, with the absence of the ground-state bleach at 400 nm and the appearance of one major absorption band at 543 nm. Moreover, its triplet excited-state lifetime deduced from the decay of the TA was 41.2 μs, which was 3 orders of magnitude longer than its emission lifetime (20 ns). This 41.2 μs lifetime was also remarkably different from those measured for the other four complexes (1−2 μs). The very long lifetime measured by TA and the resemblance of this TA spectrum to that of the dppn ligand[24] and those of other Ru(II)[39a,52] or Ir(III)[24] complexes bearing the dppn ligand suggest that the transient absorbing state observed for **5** is localized on the dppn ligand and is of $^3\pi,\pi^*$ character. The different nature of the TA state of **5** can be attributed to the more extended π-conjugation of the dppn ligand, which switches the T_1 state from the **L** ligand associated ^{3}ILCT/$^3\pi,\pi^*$ states in complexes **1**−**4** to the dppn localized $^3\pi,\pi^*$ in **5**. Such a change has been verified by our calculations of the triplet excited states for complexes **1**−**5** (Supporting Information Table S4) using the lowest triplet state at the ground-state configuration (T_1 or T_3) as the initial input wave function for analytical TDDFT of the excited state. Note that the dppn-localized $^3\pi,\pi^*$ state (T_1) in **5** is different from the emissive state (T_3) with **L**-localized $^3\pi,\pi^*$/^{3}ILCT/^{3}MLCT character. The different lifetimes deduced from TA and from emission can also be rationalized by the different nature of the transient absorbing T_1 state versus the high-lying emitting T_3 state. Although rare, Ru(II), Pt(II), and Ir(III) complexes possessing a high-lying emitting state and long-lived nonemissive transient absorbing T_1 state have been reported in the literature.[39a,52,54,55] It is also known that $[Ru(bpy)_2dppn]^{2+}$ possesses a high-lying emitting state (MLCT, 803 ns) alongside a much longer-lived (33 μs) and lower-energy nonemissive transient absorbing T_1 state.[39a]

Reverse Saturable Absorption. As the TA spectra indicated, complexes **1**−**5** all possess broad, positive triplet excited-state absorption bands in the visible to the NIR region (430−800 nm), indicative of stronger triplet excited-state absorption than the ground-state absorption in this spectral region. Thus, RSA in the visible to NIR region was anticipated for **1**−**5** and confirmed by nonlinear transmission experiments performed at 532 nm in a 2 mm cuvette on CH_3CN solutions

DOI: 10.1021/acs.inorgchem.6b02624
Inorg. Chem. 2017, 56, 3245−3259

of the complexes with 4.1 ns laser pulses. The sample concentrations were adjusted to achieve 80% linear transmission in the 2 mm cuvette at 532 nm to ensure the identical population of the singlet excited states. Under this condition, the RSA strength was determined by the excited-state absorption, which is a function of the excited-state absorption cross section and the triplet quantum yield for nanosecond excitation. The transmission versus incident energy curves for **1**−**5** are shown in Figure 4. With the increased incident energy,

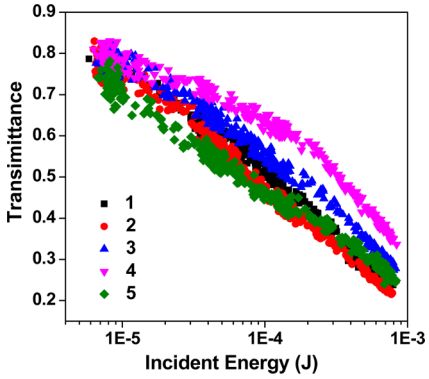

Figure 4. Transmission vs incident energy curves for complexes **1**−**5** in CH_3CN in a 2 mm cuvette for 532 nm laser pulses. The linear transmission of the solution was 80% in the 2 mm cuvette. The radius of the laser beam at the focal point was ∼96 μm.

the transmissions of **1**−**5** decreased drastically, which is a clear indication of the occurrence of RSA. The strength of RSA decreased in the order of **2** ≥ **1** ≈ **5** > **3** > **4**, and the RSA strength of **1**, **2**, and **5** was comparable to that of our best Pt(II) and Ir(III) diimine complexes reported previously.[40b,54,56]

To rationalize the observed RSA trend, the ratios of the excited-state absorption cross sections (σ_{ex}) relative to those of the ground-state (σ_0), which is the key parameter to determine the strength of RSA, were estimated according to the method described previously by our group,[56a] and the results are depicted in Table 2. The σ_0 values were deduced from the ε

Table 2. Ground-State (σ_0) and Excited-State (σ_{ex}) Absorption Cross Sections of 1−5 in CH_3CN at 532 nm

	1	2	3	4	5
$\sigma_0/1 \times 10^{-18}$ cm^2	6.9	5.2	6.6	11.0	12.8
$\sigma_{ex}/1 \times 10^{-18}$ cm^2	95	71	80	106	NA
σ_{ex}/σ_0	13.8	13.7	12.1	9.5	NA

values at 532 nm from the UV−vis absorption spectra using the conversion equation $\sigma = 2303\varepsilon/N_A$ (N_A = Avogadro's constant). The excited-state absorption cross section (σ_{ex}) was obtained from the respective ΔOD values at 532 nm and at the TA band maximum immediately after the laser excitation (i.e., determined from the TA spectrum at zero-time delay) as well as the $\varepsilon_{T1\text{-}Tn}$ at the TA band maximum. There is no bleaching band in the TA spectrum of **5**; thus, the σ_{ex} value was unable to be estimated by the singlet depletion method.[45] The trend of the estimated σ_{ex}/σ_0 ratios matched well with the observed RSA trend. The σ_{ex} values were comparable for complexes **1**−**4**; thus, the σ_0 values play the major role in determining the σ_{ex}/σ_0 ratios. For complex **5**, although its σ_{ex} value cannot be estimated by the singlet depletion method due to the lack of bleaching band in its TA spectrum, the ΔOD value at 532 nm appeared to be the largest (∼0.022) in comparison to those of complexes **1**−**4**. Consequently, even if **5** has the largest σ_0 at 532 nm, its even larger σ_{ex} renders it a strong reverse saturable absorber. Moreover, the larger σ_0 of **5** reduced the threshold of RSA, which allows RSA to occur at lower incident fluence and is a desirable feature for RSA materials. Meanwhile, complex **5** possesses the widest optical window (430−850 nm)—the spectral region where a material exhibits weak ground-state absorption but strong excited-state absorption—in the visible to the NIR region for RSA materials reported to date and retained the long-lived absorbing T_1 state. Both features make it a very promising broadband RSA material. Complex **4** also has the potential to be a broadband RSA material due to its broad optical window (430−850 nm), although its RSA is not the strongest at 532 nm among this series of complexes.

Photodynamic Therapy. We previously reported the cytotoxicity and photocytotoxicity profiles in human leukemia cells (HL60) for model complexes $[Ru(bpy)_2(N\text{^}N)]^{2+}$, where N^N = phen, tatp, dppz, or dppn.[39b] In those studies, dppn was shown to be a critical ligand of the complex for generating potent light cytotoxicities with both broadband visible and red (625 nm) light. Reduction of the π-expanded ring system by just one fused benzene ring (i.e., dppz) completely abrogated these desirable effects. Therefore, we postulated that the dppn ligand might result in complex **5** having the best photobiological profile of the present series **1**−**5**.

The dark and light cytotoxicities, quantified as the effective concentration to reduce cell viability to 50% (EC_{50}), were determined for complexes **1**−**5** in two cancer cell lines and under three conditions (in the dark, with broadband visible light illumination, and with red light-emitting diode illumination at 625 nm; Table 3 and Figure 5). Human leukemia (HL60) and skin melanoma (SKMEL28) cell lines were employed, and the light treatments consisted of 100 J cm^{-2} delivered 16 h after the cells were dosed with PS. The photocytotoxicity indices (PIs) were calculated as ratios of dark to light EC_{50} values in the two cell lines. Small light EC_{50} values combined with larger dark EC_{50} values yield large PIs and are the preferred characteristics for a potential PDT agent. Of course, additional factors are important in longer-term development (e.g., water and saline solubility, processability, chemical stability, etc.).

The cytotoxicities of **1**−**5** in the absence of a light stimulus were minimal. Complexes **3** and **4** in SKMEL28 cells gave the smallest dark EC_{50} values at 85 and 47 μM, respectively, and complexes **1**, **2**, and **5** were completely nontoxic toward both cell lines (dark EC_{50} > 100 μM). In the SKMEL28 melanoma cell line dark cytotoxicity decreased in the order of **4** > **3** > **5** > **2** > **1**, with **1** being the least toxic. In HL60 leukemia cells, the differences were less pronounced but followed the order of **4** > **5** ≈ **3** > **1** ≈ **2**, with **1** and **2** being the least toxic. Complex **5** appeared to be the least sensitive to the cell line employed in terms of its dark EC_{50} values. In general, the dark EC_{50} values were slightly smaller for SKMEL28 cells, but this difference was not substantial enough to render the complexes selective in the dark for one cell line over the other. Overall, the results indicate that this new series of PSs does not produce significant toxicity toward these cell lines without a light trigger.

With visible light activation, EC_{50} values ranged from 3.8 to 8.4 μM in SKMEL28 cells and from 8.2 to 48 μM in HL60 cells. With red light activation, these ranges were 10−204 and 30−300 μM in SKMEL28 and HL60 cells, respectively. These

DOI: 10.1021/acs.inorgchem.6b02624
Inorg. Chem. 2017, 56, 3245−3259

Table 3. (Photo)cytotoxicity of Complexes 1−5 toward SKMEL28 and HL60 Cells

		dark	vis PDT		red PDT	
		EC_{50} (μM)	EC_{50} (μM)	PI	EC_{50} (μM)	PI
SKMEL28	1	298 ± 9.62	5.16 ± 0.04	58	128 ± 4.58	2.3
	2	226 ± 5.63	5.16 ± 0.06	44	204 ± 6.82	1.1
	3	84.5 ± 2.42	8.43 ± 0.10	10	19.1 ± 0.98	4.4
	4	47.1 ± 1.51	7.91 ± 0.12	6.0	10.9 ± 0.56	4.3
	5	123 ± 3.62	3.77 ± 0.18	33	9.96 ± 0.16	12
HL60	1	>300	48.1 ± 1.40	>6.2	142 ± 51.9	>2.1
	2	>300	22.5 ± 0.99	>13	>300	*a*
	3	146 ± 37.8	14.6 ± 0.99	10	38.2 ± 4.00	3.8
	4	96.2 ± 10.9	8.21 ± 0.17	12	30.1 ± 1.76	3.2
	5	143 ± 4.25	10.3 ± 0.26	14	126 ± 9.47	1.1

[a]Not determined due to decreased solubility of complexes at high concentration.

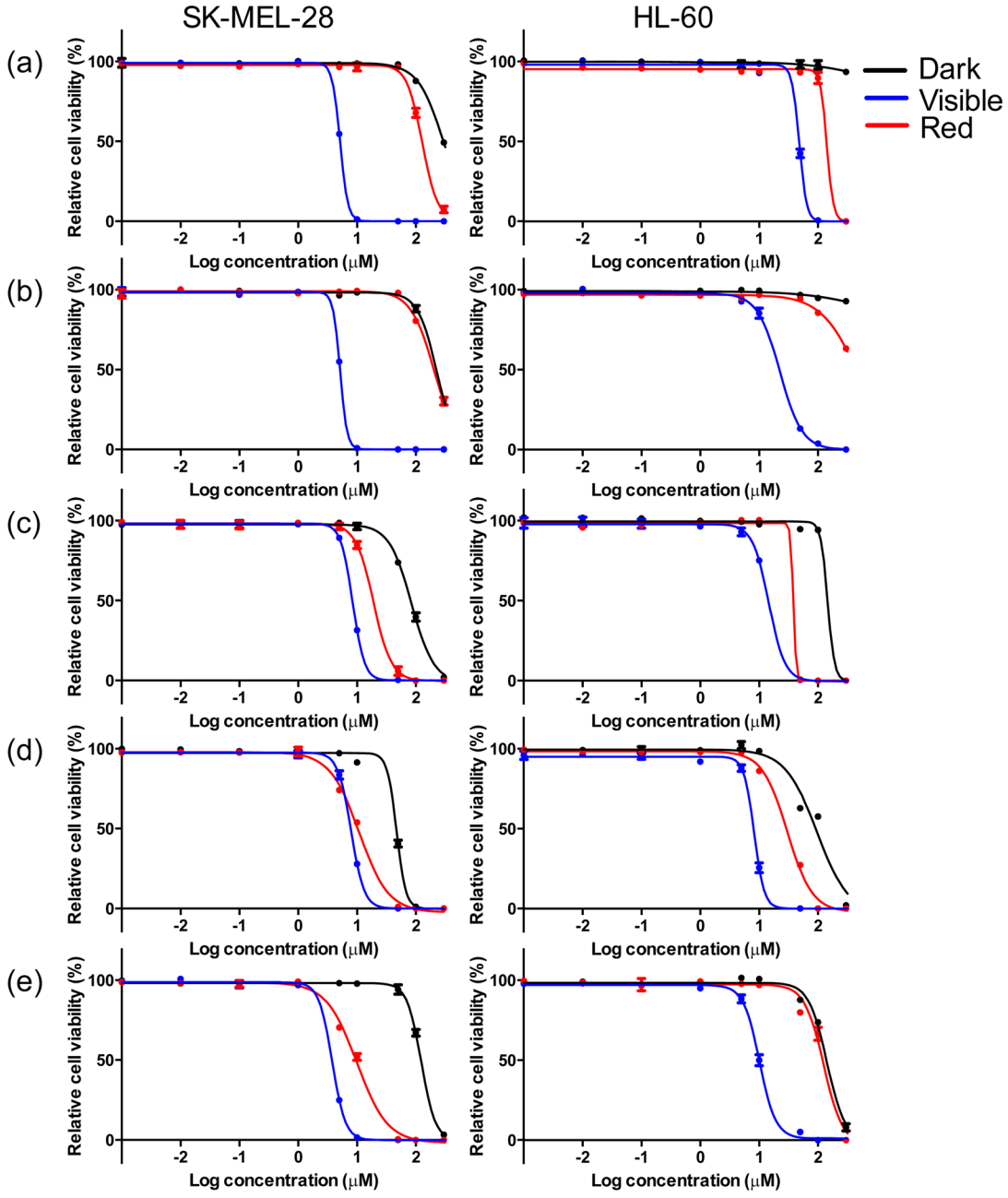

Figure 5. In vitro dose−response curves for complexes **1**−**5** (a−e) in SKMEL28 cells (left column) and HL60 cells (right column) in the dark (black) or with visible (blue) or red (red) light activation of 100 J cm^{-2}.

DOI: 10.1021/acs.inorgchem.6b02624
Inorg. Chem. 2017, 56, 3245−3259

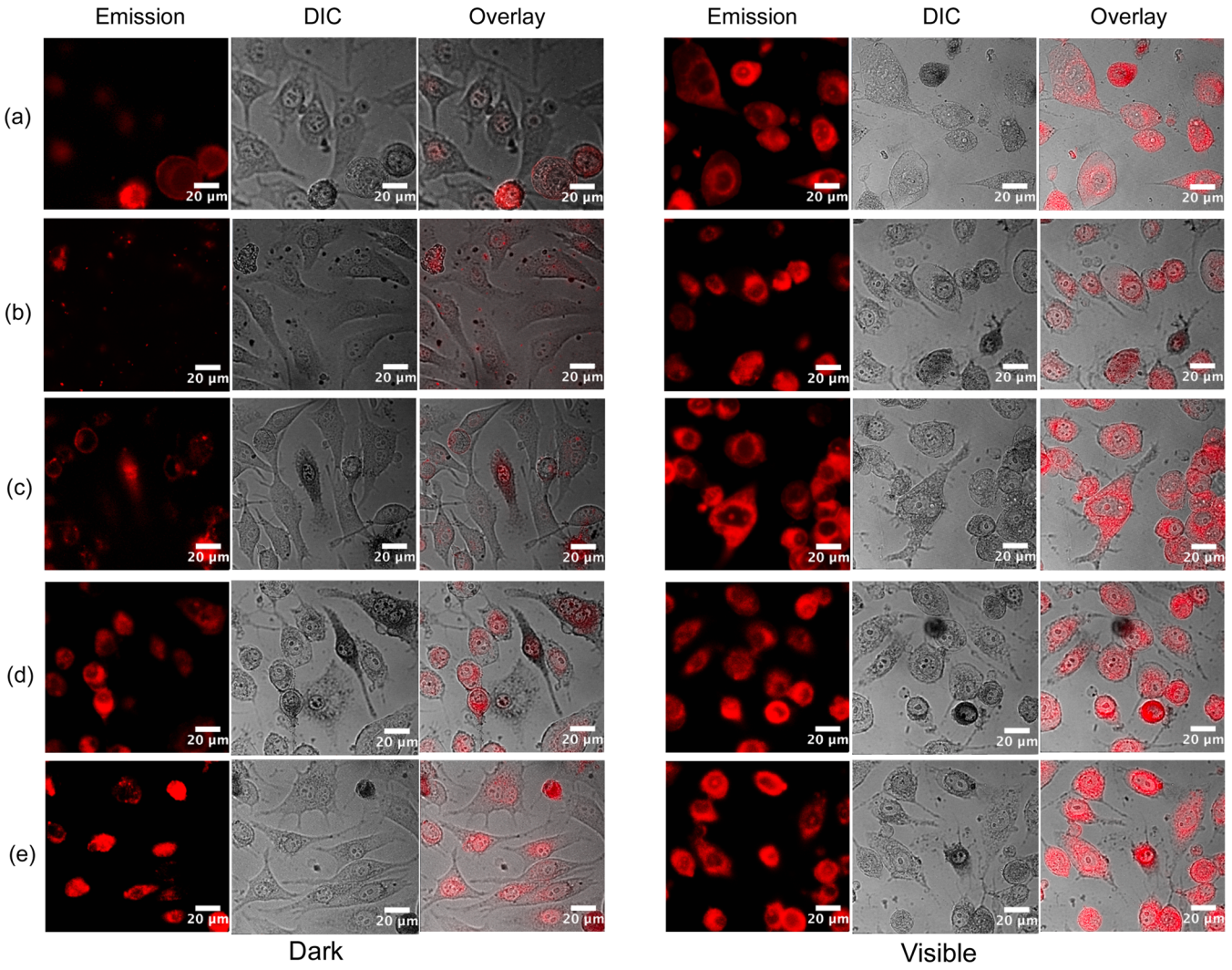

Figure 6. Confocal luminescence images of SKMEL28 cells treated with 50 μM complexes **1**−**5** (a−e) in the dark (left) or with visible light of 50 J cm^{-2} (right).

results indicate that the PSs were generally more light cytotoxic toward melanoma cells. Visible-light EC_{50} values measured for the PSs in SKMEL28 cells decreased in the order of **3** ≈ **4** > **1** ≈ **2** > **5**, with **5** being the most potent light-triggered cytotoxin. This trend differed in HL60 cells (**1** > **2** > **3** > **5** > **4**), where complex **4** was slightly more potent than **5**, and **1** and **2** were noticeably less potent. Notably, **1** was almost 10-fold more potent toward SKMEL28 cells specifically, and **2** exhibited over four-fold selectivity for melanoma cells with a visible PDT treatment. These overall trends changed with red-light PDT. When PSs were activated by red light in SKMEL28 cells, potency increased in the order of **2** < **1** < **3** < **4** ≈ **5**, while this order changed substantially in HL60 cells (**2** < **1** < **5** < **3** < **4**). **5** exhibited a high photocytotoxicity selectivity factor (SF, defined as the ratio of light EC_{50} values measured in HL60 and SKMEL28 cells, respectively) of 13 for melanoma cells with the red PDT treatment.

While there was no systematic trend relating increased π-conjugation to increased light cytotoxicity in cells as we have previously observed in model systems, it was generally the case that the most π-expansive systems **4** and **5** were the most potent in vitro PDT agents and the least π-expansive PSs **1** and **2** were the least potent regardless of cell line. The exception was that **4** displayed less activity toward SKMEL28 cells when triggered by visible light.

Of interest for clinical applications is the PI, which is a measure of the therapeutic margin. The larger the PI, the more likely it is that a given PS will have minimal off-site toxicity at the administered drug dose. PI values ranged from 1 (no PDT effect) to 58 for this series of complexes. The largest PI was measured for **1** (PI = 58) with visible PDT delivered to SKMEL28 cells. Complex **5** had the largest PIs for red in vitro PDT in SKMEL28 cells (PI = 12) and for visible in vitro PDT in HL60 cells (PI = 14). As expected for lower photon energy excitation, red PDT gave rise to less potency across both cell lines when compared to visible-light irradiation, and the corresponding PI values were also smaller. Given that red light is currently employed for clinical applications using Photofrin as the PS, it is noteworthy that complex **5** from this series is as phototoxic with red light toward cells as Photofrin but with three-fold less dark toxicity and a larger therapeutic margin (albeit in a different cancer cell line).[57] Interestingly, of the five complexes studied under these conditions, **5** exhibited the most selectivity (more than 10-fold) toward melanoma cells.

DOI: 10.1021/acs.inorgchem.6b02624
Inorg. Chem. 2017, 56, 3245−3259

The phosphorescence from **1**−**5** could be used to image cellular accumulation before and after an in vitro PDT treatment (Figure 6). While differences in phosphorescence quantum yields across the series and anticipated differential effects of the cellular environment on this luminescence preclude direct correlations between uptake and cytotoxicity, it is possible to discern qualitative aspects such as uptake and localization. Cellular uptake could be detected for all of the complexes with and without a light trigger. In all cases the uptake (as judged by luminescence intensity) was much greater after illumination (i.e., PDT-induced uptake) as would be expected with initial photo-reactions at the cell surface that compromise membrane integrity. Prior to irradiation, the PSs appeared to localize in the nucleus although increased nuclear uptake in the dark did not necessarily cause increased dark cytotoxicity as might be expected. Irradiation caused relocalization of some of the PSs to the cytoplasm, although a significant quantity remained in the nucleus. While these results do not point to one particular mode of cell death, one contributing mechanism of action could be photactivated damage to nuclear DNA. It is worth noting that the bright intracellular luminescence is a key advantage in creating *theranostic* PDT agents, that is, agents that possess diagnostic capabilities in addition to therapeutic potential.

Complexes **1**−**5** were probed for their DNA interactions using an agarose gel electrophoretic assay. Since a detectable amount of the PSs was present in the nucleus before and after illumination, DNA could serve as an intracellular target for some of the observed photocytotoxicity. Briefly, topological changes to plasmid DNA caused by interactions with exogenous agents can be discerned by changes in the electrophoretic mobility of the plasmid through the gel as a function of different treatment conditions. The migration pattern provides information on DNA binding (e.g., intercalation) and damage (e.g., unwinding, aggregation, single- or double-strand breaks) by the PS. The relative migration distances of plasmid DNA increase in the order: condensed/aggregated (Form IV, induced aggregation or condensation) < nicked circular (Form II, single-strand breaks) < linear (Form III, two single-strand breaks in close proximity or frank double-strand breaks) < supercoiled (Form I, no strand scission). Ru(II) complexes with π-expansive ligands have been shown to bind to DNA through intercalation between hydrophobic base pairs and induce single-strand breaks when irradiated with visible light.[39b]

All of the complexes of this study caused condensation of plasmid DNA in a concentration-dependent manner regardless of whether a light treatment was applied (Figure 7). This interpretation is based on the retarded migration of condensed DNA under similar electrophoretic conditions previously confirmed by atomic force microscopy.[58−60] With increasing π-conjugation of the N^N ligand on going from **1** to **5**, the DNA bands of all DNA forms became much dimmer. This attenuation in fluorescence of the ethidium dye indicator was greatest for complex **5**, where bands were barely visible across the entire concentration range of PS for the light-treated samples (Figure 7e, lanes 3−8) as well as the dark control at the highest concentration (Figure 7e, lane 9). Band disappearance has been ascribed to interference by the PS: the quenching of EtBr fluorescence, competition for EtBr binding sites, or lack of DNA intercalation by EtBr due to distortion of the helix. Regardless of which phenomenon is at play here, the gel mobility-shift assay does highlight the ability

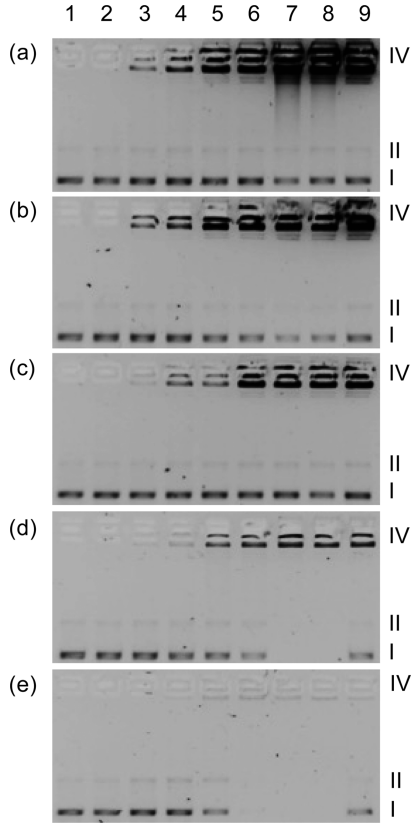

Figure 7. DNA photocleavage of pUC19 DNA (20 μM bases) dosed with Ru(II) metal complex (MC) **1** (a), **2** (b), **3** (c), **4** (d), or **5** (e) and visible light (14 J cm^{-2}). Gel mobility shift assays employed 1% agarose gels (0.75 μg mL^{-1} ethidium bromide) electrophoresed in 1X TAE at 8 V cm^{-1} for 30 min. Lane 1, DNA only (−*hν*); lane 2, DNA only (+*hν*); lane 3, 5 μM MC (+*hν*); lane 4, 20 μM MC (+*hν*); lane 5, 40 μM MC (+*hν*); lane 6, 60 μM MC (+*hν*); lane 7, 80 μM MC (+*hν*); lane 8, 100 μM MC (+*hν*); lane 9, 100 μM MC (−*hν*). Forms I, II, and IV DNA refer to supercoiled plasmid, nicked circular plasmid, and condensed/aggregated plasmid, respectively.

of **1**−**4** (and presumably **5**) to induce DNA condensation, and these PS-DNA aggregates are susceptible to DNA photodamage owing to the proximity of the PS and any reactive intermediates that it might generate upon irradiation. Given that all of the PSs investigated in the present study cause DNA condensation yet yield a wide range of dark and light cytotoxicities, we infer that these DNA interactions are not the most important factor determining the in vitro PDT effects and that DNA may not be the predominant intracellular target.

Taken together the biological studies highlight the utility of this new class of π-expansive Ru(II) complexes as theranostic PSs for PDT. While systematic trends regarding structure−activity relationships across the entire series in two cell lines under three treatment conditions did not emerge, complex **5** did demonstrate increased potency as a PDT agent with red light activation and selectivity toward melanoma cells. Current efforts are underway to determine which excited state is the most important determinant of the PDT effects and whether singlet oxygen is involved.

CONCLUSIONS

Long intrinsic lifetimes and high triplet yields are desired attributes of materials for both RSA and PDT. This study highlights the development of a new class of Ru(II) complexes

DOI: 10.1021/acs.inorgchem.6b02624
Inorg. Chem. 2017, 56, 3245−3259

in tandem for both applications. Five tris-diimine heteroleptic Ru(II) complexes **1**−**5** were synthesized, and the influence of π-conjugation of the ancillary ligands on the photophysics of the complexes was investigated by spectroscopic methods and simulated by TDDFT calculations. The lowest singlet and triplet excited states of complexes **1**−**4** were associated with the BTF-substituted phenanthroline ligand (i.e., the **L** ligand), while the lowest-energy triplet state for **5**, which bears the most π-expansive dppn ancillary ligands, was localized on dppn. The extended π-conjugation of the ancillary ligands only affected the ground-state absorption bands below 350 nm and the spin-forbidden transitions to the triplet excited states in the ranges of 500−850 nm. For complex **5**, both the S_1 and T_1 states switched to the dppn-localized π,π^* states. Although the nature of the emitting state and the emission energies of **1**−**5** are essentially the same at rt, the emission lifetimes and quantum yields decreased, as the π-conjugation of the ancillary ligands increased. Because of the same nature of the T_1 states for **1**−**4** (i.e., the **L** ligand-based ^{3}ILCT/$^3\pi,\pi^*$), their nanosecond TA spectra featured the similar shape, but the intensity of the two bands at 500 and 710 nm gradually decreased from **1** to **4** because of the increased ground-state absorption at 500−850 nm from **1** to **4**. In addition, fusing the pyrazine ring or the quinoxaline ring to the phenanthroline ancillary ligands increased the intensity of the TA band at ca. 440 nm in **3** and **4**. On the contrary, complex **5** showed the dppn ligand-based $^3\pi,\pi^*$ absorption near 540 nm with a long triplet lifetime of 41.2 μs. The RSA strength of **1**−**5** at 532 nm for nanosecond laser pulses exhibited a trend of **2** $\geq$ **1** $\approx$ **5** > **3** > **4**, which is consistent with the trend of their σ_{ex}/σ_0 ratios. The RSA strength of **1**, **2**, and **5** at 532 nm is comparable to the RSA of our best Pt(II) and Ir(III) diimine complexes reported before. Considering the widest optical window (430−850 nm) in the visible to the NIR region and the long-lived absorbing T_1 state, complex **5** appears to be a very promising broadband RSA material.

Complexes **1**−**5** also acted as PSs for PDT, with minimal cytotoxicity in the absence of a light trigger and micromolar photocytotoxicity. The structure−activity trends for the PSs with regard to dark toxicity were similar across both cell lines and did not change in a systematic manner with increasing π-conjugation on the ancillary ligands except that the least π-conjugated systems **1** and **2** were the least dark toxic to both cell lines. Visible-light PDT tended to increase with π-expansion on the ancillary ligands, with a few notable exceptions where **4** was more potent than **5**. Complex **5** exhibited the largest PI with the most clinically relevant light treatment (i.e., red light) and was over 10 times more photoselective for melanoma cells. All of the PSs luminesced in cells before and after irradiation, with signals becoming much brighter after PDT. For both conditions, the luminescence increased with increasing π-expansion despite cell-free luminescence quantum yields that diminished in this order. Confocal imaging indicated that all of the PSs were taken up by cells and penetrated the nucleus, with distribution throughout the cytosol and nucleus after irradiation. This intracellular luminescence is a convenient diagnostic tool that makes these complexes useful as *theranostic* agents. According to cell-free gel electrophoretic analysis, the complexes caused DNA to condense/aggregate in a concentration-dependent manner that was independent of π-conjugation. Therefore, this PS-DNA interaction does not appear to be responsible for the dark and light cytotoxicity differences within the series and across the two cell lines investigated. Interference with ethidium fluorescence precluded any correlations between DNA damage and π-conjugation by gel electrophoresis. Future studies are aimed at delineating the intracellular target(s) and mechanism of photobiological action for this new class of PSs and further optimizing their photosensitizing capacities for PDT.

■ ASSOCIATED CONTENT

Supporting Information

The Supporting Information is available free of charge on the ACS Publications website at DOI: 10.1021/acs.inorgchem.6b02624.

Computational methods for geometry optimizations and simulation of the electronic absorption spectra and emission energies, experimental details for cell culture, cytotoxicity and photocytotoxicity study, DNA photocleavage assays, and confocal microscopy, comparison of the experimental and simulated spectra, solvent-dependent UV−vis absorption and emission spectra, natural transition orbitals (NTOs), emission data in different solvents, excitation spectra of **5**, comparison of the normalized emission spectra of **1**−**5** in BuCN at r.t. and 77 K, time-resolved nanosecond TA spectra of **1**−**5** in CH_3CN and ligand **L** (with and without addition of $ZnCl_2$) in toluene (PDF)

■ AUTHOR INFORMATION

Corresponding Authors

*E-mail: Wenfang.Sun@ndsu.edu. Phone: +1 701-231-6254. Fax: +1 701-231-8831. (W.S.)

*E-mail: samcfarl@uncg.edu or sherri.mcfarland@acadiau.ca. Phone: +1 336-256-1080. Fax: +1 336-334-5402. (S.A.M.)

ORCID

Svetlana Kilina: 0000-0003-1350-2790

Wenfang Sun: 0000-0003-3608-611X

Notes

The authors declare no competing financial interest.

■ ACKNOWLEDGMENTS

W. Sun acknowledges the financial support from the Army Research Laboratory (W911NF-10-2-0055) for the synthesis and photophysical studies of the complexes reported in this paper. S. McFarland acknowledges financial support from the Natural Sciences and Engineering Council of Canada (NSERC), the Canadian Institutes of Health Research (CIHR), the Canadian Foundation for Innovation (CFI), and the Nova Scotia Research and Innovation Trust (NSRIT) for the photobiological studies. The computational part of the work was supported by NSF (DMR-1411086 and CNS-1229316) to W. Sun and S. Kilina. S. Kilina also acknowledges the Center for Computationally Assisted Science and Technology (CCAST) at North Dakota State University for computer access and administrative support.

■ REFERENCES

(1) Al-Rawashdeh, N. A. F.; Chatterjee, S.; Krause, J. A.; Connick, W. B. Ruthenium Bis-diimine Complexes with a Chelating Thioether Ligand: Delineating 1,10-Phenanthrolinyl and 2,2′-Bipyridyl Ligand Substituent Effects. *Inorg. Chem.* **2014**, *53*, 294−307.

(2) Kuss-Petermann, M.; Wenger, O. S. Electron Transfer Rate Maxima at Large Donor−Acceptor Distances. *J. Am. Chem. Soc.* **2016**, *138*, 1349−1358.

DOI: 10.1021/acs.inorgchem.6b02624
Inorg. Chem. 2017, 56, 3245−3259

(3) Bonn, A. G.; Yushchenko, O.; Vauthey, E.; Wenger, O. S. Photoinduced Electron Transfer in an Anthraquinone−$[Ru(bpy)_3]^{2+}$−Oligotriarylamine−$[Ru(bpy)_3]^{2+}$−Anthraquinone Pentad. *Inorg. Chem.* **2016**, *55*, 2894−2899.
(4) Costa, R. D.; Ortí, E.; Bolink, H. J.; Monti, F.; Accorsi, G.; Armaroli, N. Luminescent Ionic Transition-Metal Complexes for Light-Emitting Electrochemical Cells. *Angew. Chem., Int. Ed.* **2012**, *51*, 8178−8211.
(5) Nemati Bideh, B.; Roldan-Carmona, C.; Shahroosvand, H.; Nazeeruddin, M. K. Low-voltage, High-brightness and Deep-red Light-emitting Electrochemical Cells (LECs) Based on New Ruthenium(ii) Phenanthroimidazole Complexes. *Dalton Trans.* **2016**, *45*, 7195−7199.
(6) Lincoln, R.; Kohler, L.; Monro, S.; Yin, H.; Stephenson, M.; Zong, R.; Chouai, A.; Dorsey, C.; Hennigar, R.; Thummel, R. P.; McFarland, S. A. Exploitation of Long-Lived ^{3}IL Excited States for Metal−Organic Photodynamic Therapy: Verification in a Metastatic Melanoma Model. *J. Am. Chem. Soc.* **2013**, *135*, 17161−17175.
(7) Chou, C.-C.; Hu, F.-C.; Yeh, H.-H.; Wu, H.-P.; Chi, Y.; Clifford, J. N.; Palomares, E.; Liu, S.-H.; Chou, P.-T.; Lee, G.-H. Highly Efficient Dye-Sensitized Solar Cells Based on Panchromatic Ruthenium Sensitizers with Quinolinylbipyridine Anchors. *Angew. Chem., Int. Ed.* **2014**, *53*, 178−183.
(8) Funaki, T.; Funakoshi, H.; Kitao, O.; Onozawa-Komatsuzaki, N.; Kasuga, K.; Sayama, K.; Sugihara, H. Cyclometalated Ruthenium(II) Complexes as Near-IR Sensitizers for High Efficiency Dye-Sensitized Solar Cells. *Angew. Chem., Int. Ed.* **2012**, *51*, 7528−7531.
(9) Aiki, S.; Kijima, Y.; Kuwabara, J.; Taketoshi, A.; Koizumi, T.-A.; Akine, S.; Kanbara, T. Ligand Modification of Cyclometalated Ruthenium Complexes in the Aerobic Oxidative Dehydrogenation of Imidazolines. *ACS Catal.* **2013**, *3*, 812−816.
(10) Taketoshi, A.; Tsujimoto, A.; Maeda, S.; Koizumi, T.; Kanbara, T. Aerobic Oxidative Dehydrogenation of 2-Substituted Imidazolines Promoted by a Cyclometalated Ruthenium Catalyst. *ChemCatChem* **2010**, *2*, 58−60.
(11) Zhang, Y.; Liu, Z.; Yang, K.; Zhang, Y.; Xu, Y.; Li, H.; Wang, C.; Lu, A.; Sun, S. A Ruthenium(II) Complex as Turn-on Cu(II) Luminescent Sensor Based on Oxidative Cyclization Mechanism and Its Application in vivo. *Sci. Rep.* **2015**, *5*, 8172.
(12) Langton, M. J.; Marques, I.; Robinson, S. W.; Félix, V.; Beer, P. D. Iodide Recognition and Sensing in Water by a Halogen-Bonding Ruthenium(II)-Based Rotaxane. *Chem. - Eur. J.* **2016**, *22*, 185−192.
(13) Zhu, Y.; Gu, C.; Tang, S.; Fei, T.; Gu, X.; Wang, H.; Wang, Z.; Wang, F.; Lu, D.; Ma, Y. A New Kind of Peripheral Carbazole Substituted Ruthenium(II) Complexes for Electrochemical Deposition Organic Light-Emitting Diodes. *J. Mater. Chem.* **2009**, *19*, 3941−3949.
(14) Li, F.; Collins, J. G.; Keene, F. R. Ruthenium Complexes as Antimicrobial Agents. *Chem. Soc. Rev.* **2015**, *44*, 2529−2542.
(15) Tsui, W.-K.; Chung, L.-H.; Wong, M. M.-K.; Tsang, W.-H.; Lo, H.-S.; Liu, Y.; Leung, C.-H.; Ma, D.-L.; Chiu, S.-K.; Wong, C.-Y. Luminescent Ruthenium(II) Complex Bearing Bipyridine and N-Heterocyclic Carbene-based ĈN^C Pincer Ligand for Live-Cell Imaging of Endocytosis. *Sci. Rep.* **2015**, *5*, 9070.
(16) Coe, B. J. Developing Iron and Ruthenium Complexes for Potential Nonlinear Optical Applications. *Coord. Chem. Rev.* **2013**, *257*, 1438−1458.
(17) Knoll, J. D.; Turro, C. Control and Utilization of Ruthenium and Rhodium Metal Complex Excited States for Photoactivated Cancer Therapy. *Coord. Chem. Rev.* **2015**, *282*−*283*, 110−126.
(18) Glazer, E. C. Light-Activated Metal Complexes that Covalently Modify DNA. *Isr. J. Chem.* **2013**, *53*, 391−400.
(19) Mari, C.; Pierroz, V.; Ferrari, S.; Gasser, G. Combination of Ru(II) Complexes and Light: New Frontiers in Cancer Therapy. *Chem. Sci.* **2015**, *6*, 2660−2686.
(20) Shi, G.; Monro, S.; Hennigar, R.; Colpitts, J.; Fong, J.; Kasimova, K.; Yin, H.; DeCoste, R.; Spencer, C.; Chamberlain, L.; Mandel, A.; Lilge, L.; McFarland, S. A. Ru(II) Dyads Derived from α-Oligothiophenes: A New Class of Potent and Versatile Photosensitizers for PDT. *Coord. Chem. Rev.* **2015**, *282*−*283*, 127−138.
(21) Higgins, S. L. H.; Brewer, K. J. Designing Red-Light-Activated Multifunctional Agentsfor the Photodynamic Therapy. *Angew. Chem., Int. Ed.* **2012**, *51*, 11420−11422.
(22) Lincoln, R.; Kohler, L.; Monro, S.; Yin, H.; Stephenson, M.; Zong, R.; Chouai, A.; Dorsey, C.; Hennigar, R.; Thummel, R. P.; McFarland, S. A. Exploitation of Long-Lived ^{3}IL Excited States for Metal−Organic Photodynamic Therapy: Verification in a Metastatic Melanoma Model. *J. Am. Chem. Soc.* **2013**, *135*, 17161−17175.
(23) de Torres, M.; Semin, S.; Razdolski, I.; Xu, J.; Elemans, J. A. A. W.; Rasing, T.; Rowan, A. E.; Nolte, R. J. M. Extended π-conjugated Ruthenium Zinc-porphyrin Complexes with Enhanced Nonlinear-optical Properties. *Chem. Commun.* **2015**, *51*, 2855−2858.
(24) Wang, C.; Lystrom, L.; Yin, H.; Hetu, M.; Kilina, S.; McFarland, S. A.; Sun, W. Increasing the Triplet Lifetime and Extending the Ground-State Absorption of Biscyclometalated Ir(III) Complexes for Reverse Saturable Absorption and Photodynamic Therapy Applications. *Dalton Trans.* **2016**, *45*, 16366−16378.
(25) (a) Coe, B. J.; Jones, L. A.; Harris, J. A.; Brunschwig, B. S.; Asselberghs, I.; Clays, K.; Persoons, A. Highly Unusual Effects of π-Conjugation Extension on the Molecular Linear and Quadratic Nonlinear Optical Properties of Ruthenium(II) Ammine Complexes. *J. Am. Chem. Soc.* **2003**, *125*, 862−863. (b) Coe, B. J.; Jones, L. A.; Harris, J. A.; Brunschwig, B. S.; Asselberghs, I.; Clays, K.; Persoons, A.; Garín, J.; Orduna, J. Syntheses and Spectroscopic and Quadratic Nonlinear Optical Properties of Extended Dipolar Complexes with Ruthenium(II) Ammine Electron Donor and N-Methylpyridinium Acceptor Groups. *J. Am. Chem. Soc.* **2004**, *126*, 3880−3891. (c) Coe, B. J.; Harries, J. L.; Helliwell, M.; Jones, L. A.; Asselberghs, I.; Clays, K.; Brunschwig, B. S.; Harris, J. A.; Garín, J.; Orduna, J. Pentacyanoiron(II) as an Electron Donor Group for Nonlinear Optics: Medium-Responsive Properties and Comparisons with Related Pentaammineruthenium(II) Complexes. *J. Am. Chem. Soc.* **2006**, *128*, 12192−12204. (d) Zhang, Y.; Champagne, B. Understanding the Second-Order Nonlinear Optical Properties of One-Dimensional Ruthenium(II) Ammine Complexes. *J. Phys. Chem. C* **2013**, *117*, 1833−1848.
(26) (a) McDonagh, A. M.; Humphrey, M. G.; Samoc, M.; Luther-Davies, B. Organometallic Complexes for Nonlinear Optics. 17.[1] Synthesis, Third-Order Optical Nonlinearities, and Two-Photon Absorption Cross Section of an Alkynylruthenium Dendrimer. *Organometallics* **1999**, *18*, 5195−5197. (b) McDonagh, A. M.; Humphrey, M. G.; Samoc, M.; Luther-Davies, B.; Houbrechts, S.; Wada, T.; Sasabe, H.; Persoons, A. Organometallic Complexes for Nonlinear Optics. 16. Second and Third Order Optical Nonlinearities of Octopolar Alkynylruthenium Complexes. *J. Am. Chem. Soc.* **1999**, *121*, 1405−1406. (c) Hurst, S. K.; Humphrey, M. G.; Isoshima, T.; Wostyn, K.; Asselberghs, I.; Clays, K.; Persoons, A.; Samoc, M.; Luther-Davies, B. Organometallic Complexes for Nonlinear Optics. 28. Dimensional Evolution of Quadratic and Cubic Optical Nonlinearities in Stilbenylethynylruthenium Complexes. *Organometallics* **2002**, *21*, 2024−2026. (d) Powell, C. E.; Humphrey, M. G. Nonlinear Optical Properties of Transition Metal Acetylides and Their Derivatives. *Coord. Chem. Rev.* **2004**, *248*, 725−756. (e) Green, K. A.; Cifuentes, M. P.; Samoc, M.; Humphrey, M. G. Syntheses and NLO Properties of Metal Alkynyl Dendrimers. *Coord. Chem. Rev.* **2011**, *255*, 2025−2038. (f) Grelaud, G.; Cifuentes, M. P.; Paul, F.; Humphrey, M. G. Group 8 Metal Alkynyl Complexes for Nonlinear Optics. *J. Organomet. Chem.* **2014**, *751*, 181−200.
(27) Jiang, C.-W.; Chao, H.; Li, R.-H.; Li, H.; Ji, L.-N. Syntheses, Characterization and Third-order Nonlinear Optical Properties of Ruthenium(II) Complexes Containing 2-phenylimidazo-[4,5-*f*][1,10]-phenanthroline and Extended Diimine Ligands. *Polyhedron* **2001**, *20*, 2187−2193.
(28) (a) Girardot, C.; Lemercier, G.; Mulatier, J. C.; Chauvin, J.; Baldeck, P. L.; Andraud, C. Novel Ruthenium(II) and Zinc(II) Complexes for Two-photon Absorption Related Applications. *Dalton Trans.* **2007**, 3421−3426. (b) Girardot, C.; Cao, B.; Mulatier, J.-C.; Baldeck, P. L.; Chauvin, J.; Riehl, D.; Delaire, J. A.; Andraud, C.; Lemercier, G. Ruthenium(II) Complexes for Two-Photon Absorption-

DOI: 10.1021/acs.inorgchem.6b02624
Inorg. Chem. 2017, 56, 3245−3259

Based Optical Power Limiting. *ChemPhysChem* **2008**, *9*, 1531−1535. (c) Four, M.; Riehl, D.; Mongin, O.; Blanchard-Desce, M.; Lawson-Daku, L. M.; Moreau, J.; Chauvin, J.; Delaire, J. A.; Lemercier, G. A Novel Ruthenium(II) Complex for Two-Photon Absorption-based Optical Power Limiting in the Near-IR Range. *Phys. Chem. Chem. Phys.* **2011**, *13*, 17304−17312.

(29) Zhao, H.; Simpson, P. V.; Barlow, A.; Moxey, G. J.; Morshedi, M.; Roy, N.; Philip, R.; Zhang, C.; Cifuentes, M. P.; Humphrey, M. G. Syntheses, Spectroscopic, Electrochemical, and Third-Order Nonlinear Optical Studies of a Hybrid Tris{ruthenium(alkynyl)/(2-phenylpyridine)}iridium Complex. *Chem. - Eur. J.* **2015**, *21*, 11843−11854.

(30) Li, C.; Zhang, L.; Wang, R.; Song, Y.; Wang, Y. Dynamics of Reverse Saturable Absorption and All-optical Switching in C_{60}. *J. Opt. Soc. Am. B* **1994**, *11*, 1356−1360.

(31) Penzkofer, A. Passive Q-switching and Mode-locking for the Generation of Nanosecond to Femtosecond Pulses. *Appl. Phys. B: Photophys. Laser Chem.* **1988**, *46*, 43−60.

(32) Speiser, S.; Orenstein, M. Spatial Light Modulation via Optically Induced Absorption Changes Inmolecules. *Appl. Opt.* **1988**, *27*, 2944−2948.

(33) Band, Y. B.; Harter, D. J.; Bavli, R. Optical Pulse Compressor Composed of Saturable and Reverse Saturable Absorbers. *Chem. Phys. Lett.* **1986**, *126*, 280−284.

(34) Hirata, S.; Totani, K.; Yamashita, T.; Adachi, C.; Vacha, M. Large Reverse Saturable Absorption under Weak Continuous Incoherent Light. *Nat. Mater.* **2014**, *13*, 938−946.

(35) Dougherty, T. J.; Gomer, C. J.; Henderson, B. W.; Jori, G.; Kessel, D.; Korbelik, M.; Moan, J.; Peng, Q. Photodynamic Therapy. *J. Natl. Cancer. Inst.* **1998**, *90*, 889−905.

(36) Bonnett, R. *Chemical Aspects of Photodynamic Therapy;* Gordon and Breach Science Publishers: London, England, 2000.

(37) (a) Knoll, J. D.; Turro, C. Control and Utilization of Ruthenium and Rhodium Metal Complex Excited States for Photoactivated Cancer Therapy. *Coord. Chem. Rev.* **2015**, *282*−*283*, 110−126. (b) Mari, C.; Pierroz, V.; Ferrari, S.; Gasser, G. Combination of Ru(ii) Complexes and Light: New Frontiers in Cancer Therapy. *Chem. Sci.* **2015**, *6*, 2660−2686.

(38) (a) Howerton, B. S.; Heidary, D. K.; Glazer, E. C. Strained Ruthenium Complexes Are Potent Light-Activated Anticancer Agents. *J. Am. Chem. Soc.* **2012**, *134*, 8324−8327. (b) Sainuddin, T.; Pinto, M.; Yin, H.; Hetu, M.; Colpitts, J.; McFarland, S. A. Strained Ruthenium Metal−Organic Dyads as Photocisplatin Agents with Dual Action. *J. Inorg. Biochem.* **2016**, *158*, 45−54. (c) Wachter, E.; Howerton, B. S.; Hall, E. C.; Parkin, S.; Glazer, E. C. A New Type of DNA "Light-Switch": A Dual Photochemical Sensor and Metalating Agent for Duplex and G-quadruplex DNA. *Chem. Commun.* **2014**, *50*, 311−313.

(39) (a) Sun, Y.; Joyce, L. E.; Dickson, N. M.; Turro, C. Efficient DNA Photocleavage by $[Ru(bpy)_2(dppn)]^{2+}$ with Visible Light. *Chem. Commun.* **2010**, *46*, 2426−2428. (b) Yin, H.; Stephenson, M.; Gibson, J.; Sampson, E.; Shi, G.; Sainuddin, T.; Monro, S.; McFarland, S. A. *In Vitro* Multiwavelength PDT with ^{3}IL States: Teaching Old Molecules New Tricks. *Inorg. Chem.* **2014**, *53*, 4548−4559. (c) Stephenson, M.; Reichardt, C.; Pinto, M.; Wächtler, M.; Sainuddin, T.; Shi, G.; Yin, H.; Monro, S.; Sampson, E.; Dietzek, B.; McFarland, S. A. Ru(II) Dyads Derived from 2-(1-Pyrenyl)-1H-imidazo[4,5-*f*][1,10]phenanthroline: Versatile Photosensitizers for Photodynamic Applications. *J. Phys. Chem. A* **2014**, *118*, 10507−10521.

(40) (a) Li, Y.; Dandu, N.; Liu, R.; Li, Z.; Kilina, S.; Sun, W. Effects of Extended π-Conjugation in Phenanthroline (N^N) and Phenylpyridine (C^N) Ligands on the Photophysics and Reverse Saturable Absorption of Cationic Heteroleptic Iridium(III) Complexes. *J. Phys. Chem. C* **2014**, *118*, 6372−6384. (b) Pei, C.; Cui, P.; McCleese, C.; Kilina, S.; Burda, C.; Sun, W. Heteroleptic Cationic Iridium(III) Complexes Bearing Naphthalimidyl Substituents: Synthesis, Photophysics and Reverse Saturable Absorption. *Dalton Trans.* **2015**, *44*, 2176−2190.

(41) Zhang, L.; Li, B. A series of Eu(III) Emitters with A Novel Triphenylamine-derived Beta-Diketone Ligand. *J. Lumin.* **2009**, *129*, 1304−1308.

(42) Slattery, S. J.; Gokaldas, N.; Mick, T.; Goldsby, K. A. Bis(4,4′-bis(diethylamino)-2,2′-bipyridine)dichlororuthenium(III): A New Starting Material for Ruthenium Polypyridyl Complexes Exhibiting Low Redox Potentials. *Inorg. Chem.* **1994**, *33*, 3621−3624.

(43) Li, B.; Li, J.; Fu, Y.; Bo, Z. Porphyrins with Four Monodisperse Oligofluorene Arms as Efficient Red Light-Emitting Materials. *J. Am. Chem. Soc.* **2004**, *126*, 3430−3431.

(44) Suzuki, K.; Kobayashi, A.; Kaneko, S.; Takehira, K.; Yoshihara, T.; Ishida, H.; Shiina, Y.; Oishi, S.; Tobita, S. Reevaluation of Absolute Luminescence Quantum Yields of Standard Solutions using a Spectrometer with An Integrating Sphere and A Back-thinned CCD Detector. *Phys. Chem. Chem. Phys.* **2009**, *11*, 9850−9860.

(45) Carmichael, I.; Hug, G. L. Triplet−Triplet Absorption Spectra of Organic Molecules in Condensed Phases. *J. Phys. Chem. Ref. Data* **1986**, *15*, 1−250.

(46) Kumar, C. V.; Qin, L.; Das, P. K. Aromatic Thioketone Triplets and Their Quenching Behaviour towards Oxygen and Di-*t*-butylnitroxy Radical. A Laser-Flash-Photolysis Study. *J. Chem. Soc., Faraday Trans. 2* **1984**, *80*, 783−793.

(47) Firey, P. A.; Ford, W. E.; Sounik, J. R.; Kenney, M. E.; Rodgers, M. A. J. Silicon Naphthalocyanine Triplet State and Oxygen. A Reversible Energy-Transfer Reaction. *J. Am. Chem. Soc.* **1988**, *110*, 7626−7630.

(48) Viala, C.; Coudret, C. An Expeditious Route to *cis*-$Ru(bpy)_2C1_2$ (bpy = 2,2′-bipyridine) using Carbohydrates as Reducers. *Inorg. Chim. Acta* **2006**, *359*, 984−989.

(49) Martin, R. L. Natural Transition Orbitals. *J. Chem. Phys.* **2003**, *118*, 4775−4777.

(50) Pena, B.; Leed, N. A.; Dunbar, K. R.; Turro, C. Excited State Dynamics of Two New Ru(II) Cyclometallated Dyes: Relation to Cells for Solar Energy Conversion and Comparison to Conventional Systems. *J. Phys. Chem. C* **2012**, *116*, 22186−22195.

(51) (a) Peach, M. J. G.; Benfield, P.; Helgaker, T.; Tozer, D. J. Excitation Energies in Density Functional Theory: An Evaluation and a Diagnostic Test. *J. Chem. Phys.* **2008**, *128*, 044118. (b) Bokareva, O. S.; Grell, G.; Bokarev, S. I.; Kühn, O. Tuning Range-Separated Density Functional Theory for Photocatalytic Water Splitting Systems. *J. Chem. Theory Comput.* **2015**, *11*, 1700−1709.

(52) Liu, Y.; Hammitt, R.; Lutterman, D. A.; Joyce, L. E.; Thummel, R. P.; Turro, C. Ru(II) Complexes of New Tridentate Ligands: Unexpected High Yield of Sensitized $^1O_2$. *Inorg. Chem.* **2009**, *48*, 375−385.

(53) (a) Watts, R. J.; Missimer, D. Environmentally Hindered Radiationless Transitions between States of Different Orbital Parentage in Iridium(III) Complexes. Application of Rigid-matrix Induced Perturbations of the Pseudo-Jahn-Teller Potential to the Rigidochromic Effect in d^6 Metal Complexes. *J. Am. Chem. Soc.* **1978**, *100*, 5350−5357. (b) Lees, A. J. The Luminescence Rigidochromic Effect Exhibited by Organometallic Complexes: Rationale and Applications. *Comments Inorg. Chem.* **1995**, *17*, 319−346.

(54) Liu, R.; Li, Y.; Li, Y.; Zhu, H.; Sun, W. Photophysics and Nonlinear Absorption of Cyclometalated 4,6-Diphenyl-2,2′-bipyridyl Platinum(II) Complexes with Different Acetylide Ligands. *J. Phys. Chem. A* **2010**, *114*, 12639−12645.

(55) (a) Foxon, S. P.; Metcalfe, C.; Adams, H.; Webb, M.; Thomas, J. A. Electrochemical and Photophysical Properties of DNA Metallo-intercalators Containing the Ruthenium(II) Tris(1-pyrazolyl)methane Unit. *Inorg. Chem.* **2007**, *46*, 409−416. (b) Foxon, S. P.; Alamiry, M. A. H.; Walker, M. G.; Meijer, A. J. H. M.; Sazanovich, I. V.; Weinstein, J. A.; Thomas, J. A. Photophysical Properties and Singlet Oxygen Production by Ruthenium(II) Complexes of Benzo[*i*]dipyrido[3,2-a:2′,3′-c]phenazine: Spectroscopic and TD-DFT Study. *J. Phys. Chem. A* **2009**, *113*, 12754−12762.

(56) (a) Li, Y.; Liu, R.; Badaeva, E.; Kilina, S.; Sun, W. Long-lived π-Shape Platinum(II) Diimine Complexes Bearing 7-Benzothiazolyl-fluoren-2-yl Motif on the Bipyridine and Acetylide Ligands: Admixing

DOI: 10.1021/acs.inorgchem.6b02624
Inorg. Chem. 2017, 56, 3245−3259

π,π^* and Charge-Transfer Configurations. *J. Phys. Chem. C* **2013**, *117*, 5908−5918. (b) Sun, W.; Zhang, B.; Li, Y.; Pritchett, T. M.; Li, Z.; Haley, J. E. Broadband Nonlinear Absorbing Platinum 2,2′-Bipyridine Complex Bearing 2-(Benzothiazol-2′-yl)-9,9-diethyl-7-ethynylfluorene Ligands. *Chem. Mater.* **2010**, *22*, 6384−6392. (c) Liu, R.; Zhou, D.; Azenkeng, A.; Li, Z.; Li, Y.; Glusac, K. D.; Sun, W. Nonlinear Absorbing Platinum(II) Diimine Complexes: Synthesis, Photophysics, and Reverse Saturable Absorption. *Chem. - Eur. J.* **2012**, *18*, 11440−11448. (d) Liu, R.; Dandu, N.; Chen, J.; Li, Y.; Li, Z.; Liu, S.; Wang, C.; Kilina, S.; Kohler, B.; Sun, W. Influence of Different Diimine (N^N) Ligands on the Photophysics and Reverse Saturable Absorption of Heteroleptic Cationic Iridium(III) Complexes Bearing Cyclometalating 2-{3-[7-(Benzothiazol-2-yl)fluoren-2-yl]phenyl}-pyridine (ĈN) Ligands. *J. Phys. Chem. C* **2014**, *118*, 23233−23246. (e) Li, Y.; Dandu, N.; Liu, R.; Hu, L.; Kilina, S.; Sun, W. Nonlinear Absorbing Cationic Iridium(III) Complexes Bearing Benzothiazolyl-fluorene Motif on the Bipyridine (N^N) Ligand: Synthesis, Photophysics and Reverse Saturable Absorption. *ACS Appl. Mater. Interfaces* **2013**, *5*, 6556−6570.

(57) (a) Saha, S.; Mallick, D.; Majumdar, R.; Roy, M.; Dighe, R. R.; Jemmis, E. D.; Chakravarty, A. R. Structure−Activity Relationship of Photocytotoxic Iron(III) Complexes of Modified Dipyridophenazine Ligands. *Inorg. Chem.* **2011**, *50*, 2975−2987. (b) Hilmey, D. G.; Abe, M.; Nelen, M. I.; Stilts, C. E.; Baker, G. A.; Baker, S. N.; Bright, F. V.; Davies, S. R.; Gollnick, S. O.; Oseroff, A. R.; Gibson, S. L.; Hilf, R.; Detty, M. R. Water-Soluble, Core-Modified Porphyrins as Novel, Longer-Wavelength-Absorbing Sensitizers for Photodynamic Therapy. II. Effects of Core Heteroatoms and Meso-Substituents on Biological Activity. *J. Med. Chem.* **2002**, *45*, 449−461.

(58) Shi, Y.; Zhou, L.; Wang, R.; Pang, Y.; Xiao, W.; Li, H.; Su, Y.; Wang, X.; Zhu, B.; Zhu, X.; Yan, D.; Gu, H. In situ Preparation of Magnetic Nonviral Gene Vectors and Magnetofection in Vitro. *Nanotechnology* **2010**, *21*, 115103.

(59) Silva, G.; Oliveira, A.; Bitoque, D.; Silva, A.; Rosa da Costa, A. Transfection Efficiency of Chitosan and Thiolated Chitosan in Retinal Pigment Epithelium Cells: A Comparative Study. *J. Pharm. BioAllied Sci.* **2013**, *5*, 111−118.

(60) Qiu, K.; Yu, B.; Huang, H.; Zhang, P.; Huang, J.; Zou, S.; Chen, Y.; Ji, L.; Chao, H. A Dendritic Nano-Sized Hexanuclear Ruthenium-(II) Complex as a One- and Two-Photon Luminescent Tracking Non-Viral Gene Vector. *Sci. Rep.* **2015**, *5*, 10707.

DOI: 10.1021/acs.inorgchem.6b02624
Inorg. Chem. 2017, 56, 3245−3259